The metabolite BH4 controls T cell proliferation in autoimmunity and cancer

Shane J. F. Cronin[1,2], Corey Seehus[2], Adelheid Weidinger[3], Sebastien Talbot[2, 18], Sonja Reissig[4], Markus Seifert[5], Yann Pierson[6], Eileen McNeill[7], Maria Serena Longhi[8], Bruna Lenfers Turnes[9], Taras Kreslavsky[10,13], Melanie Kogler[1], David Hoffmann[1], Melita Ticevic[1], Débora da Luz Scheffer[9], Luigi Tortola[1], Domagoj Cikes[1], Alexander Jais[11], Manu Rangachari[12], Shuan Rao[1], Magdalena Paolino[13], Maria Novatchkova[10], Martin Aichinger[10], Lee Barrett[2], Alban Latremoliere[14], Gerald Wirnsberger[15], Guenther Lametschwandtner[15], Meinrad Busslinger[10], Stephen Zicha[16], Alexandra Latini[2,9], Simon C. Robson[7], Ari Waisman[4], Nick Andrews[2], Michael Costigan[2,17], Keith M. Channon[7], Guenter Weiss[5], Andrey V. Kozlov[3], Mark Tebbe[16], Kai Johnsson[6,19], Clifford J. Woolf[2*], and Josef M. Penninger[1*]

[1] IMBA, Institute of Molecular Biotechnology of the Austrian Academy of Sciences, Vienna, Austria.

[2] Department of Neurobiology, Harvard Medical School, Boston, MA 02115, USA; FM Kirby Neurobiology Center, Boston Children's Hospital, Boston, MA 02115, USA.

[3] Ludwig Boltzmann Institute for Experimental and Clinical Traumatology, AUVA Research Center, Donaueschingen Str. 13, 1200 Vienna, Austria.

[4] Institute for Molecular Medicine, University Medical Center of the Johannes Gutenberg-University Mainz, Mainz, Germany.

[5] Department of Internal Medicine II (Infectious Diseases, Immunology, Rheumatology and Pneumology), Medical University of Innsbruck, Anichstr. 35, A-6020 Innsbruck, Austria.

[6] Institute of Chemical Sciences and Engineering, Institute of Bioengineering, National Centre of Competence in Research (NCCR) in Chemical Biology, École Polytechnique Fédérale de Lausanne (EPFL), 1015 Lausanne, Switzerland

[7] Division of Cardiovascular Medicine, British Heart Foundation Centre for Research Excellence, John Radcliffe Hospital, University of Oxford, U.K., Wellcome Trust Centre for Human Genetics, Roosevelt Drive, University of Oxford, OX3 7BN, U.K.

[8] Division of Gastroenterology and Liver Center, Department of Medicine, Beth Israel Deaconess Medical Center (BIDMC) and Harvard Medical School (HMS), Harvard University, Office E/CLS 612, 3 Blackfan Circle, Boston, MA, 02115, USA.

[9] LABOX, Departamento de Bioquímica, Universidade Federal de Santa Catarina, Florianópolis, SC 88040-900, Brazil.

[10] Research Institute of Molecular Pathology, Vienna Biocenter, Campus-Vienna-Biocenter 1, Vienna, Austria.

[11] Department of Neuronal Control of Metabolism, Max Planck Institute for Metabolism Research, Cologne, Germany.

[12] Department of Neurosciences, Centre de recherche de CHU de Québec - Université Laval, Québec QC Canada, Department of Molecular Medicine, Faculty of Medicine, Université Laval, Québec QC Canada.

[13] Karolinska Institute, Department of Medicine Solna, Center for Molecular Medicine, Karolinska University Hospital Solna, 171 76 Stockholm, Sweden.

[14] Neurosurgery Department, Johns Hopkins School of Medicine, Baltimore, MD 21205, USA.

[15] Apeiron Biologics AG, Vienna, Austria.

[16] Quartet Medicine, 400 Technology Square, Cambridge, MA 01239, USA.

[17] Department of Anesthesia, Harvard Medical School, Boston, MA 02115, USA; Boston Children's Hospital, Boston, MA 02115, USA.

[18] Département de Pharmacologie et Physiologie, Université de Montréal, Montréal, QC, Canada

[19] Max-Planck Institute for Medical Research, Department of Chemical Biology, 69120 Heidelberg, Germany

*Correspondence and requests for materials should be addressed to josef.penninger@imba.oeaw.ac.at or clifford.woolf@childrens.harvard.edu

Abstract

Genetic regulators and environmental stimuli modulate T cell activation in autoimmunity and cancer. The enzyme co-factor tetrahydrobiopterin (BH4) is involved in monoamine neurotransmitter production, nitric oxide generation and pain [1,2] We now identify a fundamental role for BH4 in T cell biology. Genetic inactivation of GTP cyclohydrolase 1 (GCH1), the rate-limiting enzyme in the synthesis of BH4 and inhibition of sepiapterin reductase (SPR), the terminal enzyme in its synthetic pathway, severely impair the proliferation of mature mouse and human T cells. BH4 production in activated T cells is linked to alterations in iron metabolism and mitochondrial bioenergetics. *In vivo* blockade of BH4 synthesis abrogates T cell-mediated autoimmunity and allergic inflammation, while enhancing BH4 levels by GCH1 overexpression, augments $CD4^+$ and $CD8^+$ T cell responses increasing their anti-tumour activity *in vivo*. Administration of BH4 to mice markedly reduces tumour growth and expands intra-tumoral effector T cells. Kynurenine, a tryptophan metabolite that blocks anti-tumour immunity, inhibits T cell proliferation in a manner that can be rescued by BH4. Finally, we report development of a potent SPR antagonist for potential clinical use. Our data uncover GCH1, SPR and their downstream metabolite BH4, as critical regulators of T cell biology, which can be readily manipulated to either block autoimmunity or enhance anti-cancer immunity.

Main text

GCH1, the first enzyme in the *de nova* BH4 synthesis pathway, is expressed in activated T cells[3,4]. Using isolated $CD4^+$ and $CD8^+$ T cells from a *Gch1-Gfp* reporter mouse line[1], we confirmed that GCH1 is induced in activated T-cells in response both to PMA/ionomycin and TCR stimulation, using anti-CD3/CD28 crosslinking (Extended Data Fig. 1a-c). To explore the function of the GCH1/BH4 pathway in these cells, we generated *Gch1* T cell-specific knockout mice, crossing *Lck-Cre* driver mice with *Gch1*(fl/fl)[5] mice (*Gch1;Lck*). *Gch1;Lck* mice showed normal numbers of thymic and peripheral T cells compared to Cre-only controls (Extended Data Fig. 1d), i.e. lack of GCH1 does not influence T cell development or peripheral T cell homeostasis. Stimulation of mature peripheral $CD4^+$ T cells from *Gch1;Lck* mice revealed as expected, severely reduced GCH1 protein and BH4 production relative to controls (Fig. 1a,b). Shortly following TCR engagement (16 hours), no differences between *Gch1;Lck* and control T

cells in either surface activation marker expression or interleukin (IL)-2 secretion was observed (Fig. 1c,d). Similar results were obtained in $CD8^+$ T cells (not shown). However, TCR-stimulated *Gch1*-deficient $CD4^+$ and $CD8^+$ T cells displayed a markedly reduced proliferation (Fig. 1e,f; Extended Data Fig. 1e,f). In contrast to the anti-proliferative action on peripheral T cells, *Gch1* ablation did not affect proliferation of DN3a thymocytes co-cultured with OP9-DL1 stromal cells (Extended Data Fig. 1g-i). Moreover, there were no obvious differences in the survival of thymocytes or mature naive peripheral T cells (Extended Data Fig. 2a,b).

To validate these findings, we crossed a different T cell-specific Cre mouse line, *RORgammact Cre*[6], with *Gch1*(fl/fl)[5] mice. Again, specific loss of GCH1 in T cells did not affect thymocyte development or peripheral T cell homeostasis (data not shown). Importantly, GCH1 was again though, a critical regulator of mature T cell proliferation (Fig. 1e; Extended Data Fig. 2c,d). B cell-specific deletion of *Gch1* using *MB1-Cre*[7] did not affect B cell development or function (Extended Data Fig. 2e-h). Moreover, loss of GCH1 had no effect on peripheral Treg development, Treg numbers, or their suppressive capacity (Extended Data Fig. 3a-f). We conclude that GCH1 induction and BH4 synthesis is required for effective $CD4^+$ and $CD8^+$ T cell proliferation.

To investigate whether G*ch1*-ablated, BH4-deficent T cells are defective *in vivo*, we studied several models of T cell-dependent inflammation. In a colitis model in which naïve, $CD4^+$ T cells are transferred into *Rag1*$^{-/-}$ hosts[8] , transfer of *Gch1*-deficient $CD4^+$ T cells resulted in a substantially lower influx of immune cells with less colonic inflammation and colitis development (Fig. 1g,h). Although colonic and mesenteric lymph node $CD4^+$ T cells were significantly reduced, production of inflammatory T cell cytokines IL17A and IFNγ were apparently not affected by selective *Gch1* deletion (Extended Data Fig. 3g-i). Next, we utilized a model of type 2 allergic airway inflammation which immune cells, particularly $CD4^+$ Th2 cells and eosinophils, are central to disease pathology[9,10]. Compared to controls, *Gch1;Lck* mice showed significantly fewer $CD45^+$ cells, eosinophils, and T cells in bronchoalveolar lavage (Fig. 1i). Moreover, T cell-dependent OVA-induced immune responses were reduced during primary immunization and re-challenge (Extended Data Fig. 4a). *Gch1;Lck* mice also showed

111 significantly reduced inflammatory responses in a T cell-mediated skin dermatitis model[11] (Fig.
112 1j) and in the experimental autoimmune encephalomyelitis (EAE) model of multiple sclerosis[12,13]
113 (Extended Data Fig. 4b,c) Genetic ablation of *Gch1* in T cells alleviates, therefore, T cell-
114 mediated inflammatory intestinal, airway, skin and brain diseases.

115

116 Inhibition of GCH1 pharmacologically is challenging due to its inaccessible active sites[14,15].
117 Therefore, we utilized an inhibitor, SPRi3, that targets sepiapterin reductase (SPR), the terminal
118 enzyme in the *de novo* BH4 synthesis pathway (Fig. 2a, Extended Data Fig. 4d). Purified naïve
119 $CD4^+$ T cells treated with SPRi3 showed lower BH4 levels compared to vehicle-treated cells
120 following TCR stimulation (Fig. 2a). SPRi3-treated, TCR-stimulated $CD4^+$ and $CD8^+$ cells
121 displayed a defect in proliferation similar to that in *Gch1* genetically-ablated T cells (Fig. 2b)
122 without affecting the survival of non-stimulated T cells or the induction of early activation
123 markers (Extended Data Fig. 4e,f). EdU-pulse labelling revealed that SPRi3-treated cells and
124 *Gch1*-deficient T cells displayed significantly less S-phase cells after TCR stimulation than
125 vehicle-treated control cells, associated with increased cell death (Extended Data Fig. 4g). *In*
126 *vivo,* SPRi3 administration significantly ameliorated colitis, greatly diminishing intestinal
127 infiltration of T cells and other immune cells after $CD4^+$ T cell transfer (Fig. 2c). SPRi3 treatment
128 also reduced immune cell infiltration into the lung after an inhaled OVA challenge in sensitized
129 mice (Fig. 2d). To determine if these findings translate to human T cells, we isolated human
130 peripheral blood mononuclear cells from different healthy donors (n=4). Following anti-
131 CD3/CD28 stimulation, SPRi3-treated, freshly isolated human T cells also exhibited significantly
132 reduced proliferation compared to vehicle-treated cells (Fig. 2e). Moreover, we observed a
133 significant decrease in proliferative capacity in SPRi3-treated purified human effector $CD4^+$ T
134 cells after anti-CD3/CD8 re-stimulation (Fig. 2f).

135

136 To explore the molecular mechanisms responsible for the proliferation deficit we performed gene
137 expression profiling in TCR-stimulated $CD4^+$ T cells from control and *Gch1;Lck* mice. Analysis
138 of the significantly altered genes confirmed that loss of GCH1 did not affect early T cell
139 activation (data accessible through GEO GSE108101). Biogenic amines or their amino acid
140 precursors, for which BH4 is a co-factor[2], were also unaffected (Extended Data Fig. 4j,k;

Supplementary Table 1). Intriguingly, several genes involved in iron homeostasis or its availability were upregulated in the absence of GCH1, a finding confirmed by Western blot of activated *Gch1*-ablated T cells (Fig. 2g). Total iron levels were significantly reduced in TCR-activated *Gch1*-ablated $CD4^+$ T cells compared to control cells (Fig. 2h). As one of the most upregulated genes in *Gch1*-ablated cells was mitoferrin, a mitochondrial iron transporter and iron is critical for mitochondrial respiration[16], we analyzed the energy needs of *Gch1*-deficent activated T cells. Both *Gch1*-deficient and SPRi3-treated $CD4^+$ T cells synthesized less ATP than control cells after anti-CD3/CD28 stimulation (Extended Data Fig. 5a,b). Furthermore, both lactate and pyruvate levels were enhanced in activated *Gch1*-deficent T cells, indicating augmented glycolysis (Extended Data Fig. 5c), suggesting the loss of GCH1 expression affects mitochondrial respiration.

Following anti-CD3/CD28 stimulation, mitochondrial respiration and oxygen consumption were significantly lower in BH4-deficient T cells than control cells (Fig. 2i; Extended Data Fig. 5d-g). CytochromeC, a redox-active protein which contains heme groups that reversibly alternate between their Fe^{2+} and Fe^{3+} oxidation states is important for the mitochondrial electron transport chain (ETC) and we confirmed earlier reports[17–19] that BH4 efficiently reduces ferri-cytochromeC (CytoC-Fe^{3+}) to ferro-cytochromeC (CytoC-Fe^{2+}) at doses that are physiologic in activated T cells (Fig. 2j). Critically, we could rescue ETC function by providing reduced cytochromeC (cytoC-F^{e2+}) to BH4-deficent cells (Fig. 2k,l). Impaired ETC in activated *Gch1*-ablated and SPRi3-treated $CD4^+$ T cells was associated with elevation of superoxide reactive oxygen species (ROS) (Extended Data Fig. 6a,b). The superoxide scavenger, N-acetylcysteine (NAC) only partially rescued the proliferation defect of *Gch1*-ablated T cells and NAC addition did not rescue the iron deficiency observed in activated *Gch1*-ablated $CD4^+$ T cells nor enhance ATP production (Extended Data Fig. 6c-f), suggesting that the enhanced ROS is the result of mitochondrial dysregulation. BH4 is a co-factor for nitric oxide synthases (NOS) and is required for nitric oxide production $(NO)^2$. However, under our experimental conditions we did not observe detectable iNOS (inducible NOS) expression nor NO production until several days after T cell activation (Extended Data Fig. 6g-j). Our data indicate that antigen receptor stimulated, BH4-depleted T cells display a defective iron redox cycling of cytochromeC, which leads to mitochondrial dysfunction.

Since SPRi3 has relatively low potency and a short half-life, we developed a novel SPR inhibitor, QM385, which is structurally-distinct from SPRi3 (Fig. 3a). QM385 binds with high affinity to human SPR in a cell-free assay and efficiently reduced BH4 levels in anti-CD3/CD28 activated mouse splenocytes as well as anti-CD3/CD28 activated human PBMCs (Extended Data Fig. 7a-c). QM385 is orally bioavailable, has a long half-life (Supplementary Table 2), and reduces BH4 plasma levels dose-dependently while concurrently increasing sepiapterin levels (Fig. 3b), a sensitive biomarker of SPR inhibition[1]. QM385 showed lack of inhibition of a panel of physiologically important targets as well as closely-related reductases (Supplementary Table 3) and *in vivo* administration did not result in detectable adverse effects. QM385 treatment resulted in markedly less $CD4^+$ T cell proliferation *in vitro* (Fig. 3c). Moreover, in activated $CD4^+$ T cells, QM385 significantly reduced ETC function as well as ATP levels and led to an elevation in ROS (Extended Data Fig. 7d-f). Altogether, QM385 phenocopies the effects of SPRi3 *in vitro,* albeit at much lower concentrations. Importantly, oral administration of QM385 for three days significantly reduced the number of inflammatory T cells and eosinophils in the OVA-induced and house dust mite (HDM) airway allergic inflammation models (Fig. 3d; Extended Data Fig. 7g); which are T cell dependent[20]. QM385 effectively inhibited proliferation of human $CD4^+$ T cells at low doses (Extended Data Fig. 7h). We have, therefore, developed a novel SPR inhibitor that blocks T cell proliferation and autoimmunity at nanomolar potency with good oral bioavailability and this or similar compounds could potentially be used to treat T cell mediated autoimmune and allergic diseases.

To investigate whether an elevation of GCH1 and BH4 enhances T cell function *in vivo,* we crossed the *Lck-Cre* driver line to Cre-recombinase inducible HA-tagged human *GCH1* over-expressing mice (designated GOE)[1], generating *GOE;Lck* animals (Extended Data Fig. 8a). T cell development and homeostasis of peripheral $CD4^+$ and $CD8^+$ T cells were unaffected in these mice, though in the periphery there was a significant increase in the proportion of effector T cells (Extended Data Fig. 8b-d). Anti-CD3/CD28-stimulated $CD4^+$ T cells from the *GOE;Lck* mice had elevated BH4 levels compared to controls (Fig. 4a) and displayed enhanced proliferation upon activation (Fig. 4b). GCH1 overexpression in unstimulated naïve T cells did not result in proliferation nor any overt spontaneous autoimmunity. To validate that elevated GCH1 increases proliferation of activated T cells, we used additional T cell-specific Cre lines to drive GCH1-HA

expression – namely *CD4-Cre* and tamoxifen-inducible *ERT-Cre,* both of which enhanced T cell proliferation and cytokine production (Extended Data Fig. 8e-j). In *GOE;Lck* mice we also observed increased inflammatory cells, including T cells, in the OVA-induced allergic inflammation asthma model (Extended Data Fig. 9a) and a significantly greater severity in the *in vivo* T cell transfer colitis model (Extended Data Fig. 9b,c). Overproduction of BH4 in Tregs did not affect their suppressive function in transfer colitis (Extended Data Fig. 9d). Administration of sepiapterin to anti-CD3/CD28-stimulated $CD4^+$ T cells also elevated BH4 levels and enhanced proliferation of stimulated $CD4^+$ and $CD8^+$ T cells (Fig. 4c; Extended Data Fig. 9e-g). Furthermore, treatment of stimulated $CD4^+$ T cells with BH4 itself increased both proliferation and IL-2 secretion (Extended Data Fig. 9h,i) and the proliferative and S-phase entry defects observed in *Gch1*-ablated T cells were rescued with either sepiapterin (Extended Data Fig. 9e, f) or BH4 (Extended Data Fig. 9j). In activated *Gch1*-ablated T cells, sepiapterin supplementation also restored iron levels, reduced superoxide, and increased ATP production (Extended Data Fig. 10a-c) reinforcing that these deficits are due to reduced BH4 levels.

To address whether hyperactivation of the BH4 pathway in T cells promotes anti-cancer immunity, we orthotopically injected E0771 breast cancer cells into syngeneic mice to generate mammary tumors[21]. *GOE;CD4* mice, unlike controls, completely rejected tumor growth (Fig. 4d). Moreover, treatment of mice carrying established E0771-derived mammary tumors with BH4, slowed growth of the tumors (Fig. 4e). Tumors in BH4-treated mice displayed increased frequencies of activated effector $CD4^+$ and $CD8^+$ cells among the infiltrating T cells, compared to vehicle-treated mice (Fig. 4f; Extended Data Fig. 10d). BH4 treatment in *Rag2*$^{-/-}$ hosts had no effect on breast cancer growth, confirming that the effect of BH4 is via action on the adaptive immune system (Fig. 4g). These results were validated with a second orthotopic model, the TC-1 cancer line (Extended Data Fig. 10e-g). Kynurenine, a tryptophan metabolite inhibits T cell proliferation[22]. Interestingly, xanthurenic acid a kynurenine metabolite, blocks SPR activity[23]. We now demonstrate that kynurenine treatment inhibits SPR in activated T cells, as evident by increased sepiapterin levels (Extended Data Fig. 10h). Addition of kynurenine to T cell cultures also reduced T cell proliferation and increased ROS in activated T cells, both of which were fully restored by addition of BH4 (Fig. 4h,i; Extended Data Fig. 10i,j).

In conclusion, we reveal that BH4 is required for the effective proliferation of mature T cells *in vitro* and *in vivo* and that this is mechanistically linked to altered iron metabolism and mitochondrial respiration. Nutritional iron deficiency is associated with impaired T cell proliferation and delayed-type hypersensitivity responses, while humoral immunity is largely preserved[24,25]. Iron-deficiency anemia is also associated with increased incidence of cancer[26,27]. Importantly, we find that BH4 is required for T cell-driven autoimmunity and allergic inflammation and its inhibition by kynurenine links the immunosuppressive tumor environment to impaired T cell function. An elevation of BH4 can overcome such inhibition to enhance immunity and inhibit tumor growth. Therefore, blockade of the BH4 synthetic pathway could be a viable option to abrogate proinflammatory auto-aggressive T cells in T cell driven pathological diseases, whereas its elevation could be a novel way to enhance anti-tumor immunity.

Main text references

1. Latremoliere, A. *et al.* Reduction of Neuropathic and Inflammatory Pain through Inhibition of the Tetrahydrobiopterin Pathway. *Neuron* **86,** 1393–1406 (2015).

2. Werner, E. R., Blau, N. & Thöny, B. Tetrahydrobiopterin: biochemistry and pathophysiology. *Biochem. J.* **438,** 397–414 (2011).

3. Chen, W. *et al.* Role of increased guanosine triphosphate cyclohydrolase-1 expression and tetrahydrobiopterin levels upon T cell activation. *J. Biol. Chem.* **286,** 13846–13851 (2011).

4. Ziegler, I. *et al.* Control of tetrahydrobiopterin synthesis in T lymphocytes by synergistic action of interferon-γ and interleukin-2. *J. Biol. Chem.* **265,** 17026–17030 (1990).

5. Chuaiphichai, S. *et al.* Cell-autonomous role of endothelial GTP cyclohydrolase 1 and tetrahydrobiopterin in blood pressure regulation. *Hypertension* **64,** 530–540 (2014).

6. Eberl, G. & Littman, D. R. Thymic origin of intestinal alphabeta T cells revealed by fate mapping of RORgammat+ cells. *Science* **305,** 248–51 (2004).

7. Hobeika, E. *et al.* Testing gene function early in the B cell lineage in mb1-cre mice. *Proc. Natl. Acad. Sci.* **103,** 13789–13794 (2006).

8. Sledzińska, A. *et al.* TGF-β signalling is required for $CD4^+$ T cell homeostasis but dispensable for regulatory T cell function. *PLoS Biol.* **11,** e1001674 (2013).

9. Talbot, S. *et al.* Silencing Nociceptor Neurons Reduces Allergic Airway Inflammation. *Neuron* **87,** 341–355 (2015).

10. Haworth, O., Cernadas, M., Yang, R., Serhan, C. N. & Levy, B. D. Resolvin E1 regulates interleukin 23, interferon-γ and lipoxin A4 to promote the resolution of allergic airway inflammation. *Nat. Immunol.* **9,** 873–879 (2008).

11. Martin, S. F. *et al.* Toll-like receptor and IL-12 signaling control susceptibility to contact hypersensitivity. *J. Exp. Med.* **205,** 2151–2162 (2008).

12. Rangachari, M. & Kuchroo, V. K. Using EAE to better understand principles of immune function and autoimmune pathology. *Journal of Autoimmunity* **45,** 31–39 (2013).

13. Rangachari, M. *et al.* Bat3 promotes T cell responses and autoimmunity by repressing Tim-3–mediated cell death and exhaustion. *Nat. Med.* **18,** 1394–1400 (2012).

14. Nar, H. *et al.* Active site topology and reaction mechanism of GTP cyclohydrolase I. *Proc. Natl. Acad. Sci. U. S. A.* **92,** 12120–12125 (1995).

15. Nar, H. *et al.* Atomic structure of GTP cyclohydrolase I. *Structure* **3,** 459–466 (1995).

16. Volani, C. *et al.* Dietary iron loading negatively affects liver mitochondrial function. *Metallomics* 1634–1644 (2017). doi:10.1039/c7mt00177k

17. M. C. Archer, D. J. Vonderschmitt, K. G. S. Mechanism of Oxidation of Tetrahydropterins. *Can. J. Biochem.* **Vol. 50,** 1174–1182 (1972).

18. Eberlein, G., Bruice, T. C., Lazarus, R. A., Henrie, R. & Benkovic, S. J. The Interconversion of the 5,6,7,8-Tetrahydro-, 7,8-Dihydro-, and Radical Forms of 6,6,7,7-

Tetramethyldihydropterin. A Model for the Biopterin Center of Aromatic Amino Acid Mixed Function Oxidases. *J. Am. Chem. Soc.* **106,** 7916–7924 (1984).

19. Capeillere-Blandin, C., Mathieu, D. & Mansuy, D. Reduction of ferric haemoproteins by tetrahydropterins: a kinetic study. *Biochem. J.* **392,** 583–587 (2005).

20. Hondowicz, B. D. *et al.* Interleukin-2-Dependent Allergen-Specific Tissue-Resident Memory Cells Drive Asthma. *Immunity* **44,** 155–166 (2016).

21. Ewens, A., Mihich, E. & Ehrke, M. J. Distant metastasis from subcutaneously grown E0771 medullary breast adenocarcinoma. *Anticancer Res.* **25,** 3905–3915 (2005).

22. Curti, A. *et al.* Indoleamine 2,3-dioxygenase-expressing leukemic dendritic cells impair a leukemia-specific immune response by inducing potent T regulatory cells. *Haematologica* **95,** 2022–2030 (2010).

23. Haruki, H., Hovius, R., Pedersen, M. G. & Johnsson, K. Tetrahydrobiopterin biosynthesis as a potential target of the kynurenine pathway metabolite xanthurenic acid. *J. Biol. Chem.* **291,** 652–657 (2016).

24. Oppenheimer, S. J. Iron and its relation to immunity and infectious disease. *J. Nutr.* **131,** 616S–633S; discussion 633S–635S (2001).

25. Cassat, J. E. & Skaar, E. P. Iron in infection and immunity. *Cell Host and Microbe* **13,** 509–519 (2013).

26. Chia-Jen Liu, Kuo-Wei Chen, Yu-Wen Hu, Ying-Chung Hong, Yu-Chung Huang, T.-J. C. and C.-H. T. Chronic Iron Deficiency Anemia and Cancer Risk. *Blood* **120,** 5172 (2012).

27. Hung, N. *et al.* Risk of Cancer in Patients with Iron Deficiency Anemia: A Nationwide Population-Based Study. *PLoS One* **10,** e0119647 (2015).

Acknowledgements. We thank all members of our laboratories for helpful discussions and Life Science Editors for editorial support. We would like to thank Shanghai ChemPartners for running the drug metabolism and pharmacokinetic assays associated with QM385. J.M.P. is supported by grants from IMBA, the Austrian Ministry of Sciences, the Austrian Academy of Sciences, an ERC Advanced Grant, and an Era of Hope Innovator award. CJW is supported by an NIH R37 grant. Would also like to acknowledge the Christian Doppler Laboratory for Iron Metabolism and Anemia research as funding body of our research (MS, GW). MR is supported by EMD Serono, Canada and MS Network Transitional Career Development Award. Human studies received IRB approval (2011P000202) from Beth Israel Deaconess Medical Center Ethics Committee and written consent was obtained from all study participants prior to inclusion in the study.

Author Contributions. SJFC, together with CJW and JMP, conceived and designed the study. All experiments were performed by SJFC with the following exceptions: AW and AJ performed mitochondrial respiration analyses, SR performed colonoscopy grading, ST, CS, BLT the asthma model, CS and BLT the HDM model. YP performed the iron reduction experiment, MSL, GL, and GW performed human T cell proliferation assays. MS performed the iron measurements. TK performed *in vitro* thymocyte differentiation experiments. MN performed microarray analysis. EMN, BLT and DLS performed biopterin and sepiapterin measurements. MK, DH, MT, LT, DC, SR, MP, MA helped with the cancer studies. LB, NA, AL, MC helped with compound dosing and BH4 biology discussions. MT and SZ performed QM385 pharmacokinetic analysis. SJFC, CJW and JMP wrote the manuscript with input from all authors. The authors declare no competing financial interests.

Author information.

Competing interests. The authors declare no competing interests.

Correspondence and requests for materials should be addressed to josef.penninger@imba.oeaw.ac.at or clifford.woolf@childrens.harvard.edu

Main Figure Legends

Figure 1. BH4 pathway is indispensable for effective T cell proliferation *in vitro* and *in vivo*.

a, Immunoblot of GCH1 after 24 hour TCR stimulation in $CD4^+$ T cells. Experiment was repeated three times with similar results. **b,** BH4 production upon 24-hour anti-CD3/CD28 stimulation in purified $CD4^+$ control and *Gch1*-null T cells. Data (n=5 mice) shown as means ± s.e.m. **c d,** Representative FACS blot depicting early activation markers **(b)** and IL-2 secretion **(c)** before and after T cell stimulation (16 hours). Data (n=5 independent samples) shown as means ± s.e.m. Experiment was repeated two independent times with similar results. **e,** $CD4^+$ T cell proliferation after 3 days of stimulation from control and *Gch1;Lck* mice. Representative data from >15 experiments showing similar results. **f,** Quantification of $CD4^+$ T cell proliferation from individual *Gch1;Lck* (upper panel, n=10) and *Gch1;RORc* (lower panel, n=7) mice. Data shown as means ± s.e.m. **g, h,** Transfer colitis model of intestinal autoimmunity. **g,** Schematic outline (top) and colitis scores of transferred control and *Gch1*-ablated $CD4^+$ T cells into $Rag1^{-/-}$ hosts. Data (n=10 mice) shown as means ± s.e.m. **h,** Representative immunofluorescence depicting intestinal infiltration of various immune cells. Scale bar, 200μm. **i,** Allergic airway inflammatory disease model and quantification of inflammatory cells in bronchoalveolar lavage fluids (BALFs). Data (n=35 for control mice; n=31 for *Gch1;Lck* mice) shown as means ± s.e.m. **j,** Percentage increase of ear swelling after re-challenge using 2,4,6-trinitrochlorobenzene (TNCB)-dependent skin hypersensitivity model. Data shown as means ± s.e.m. n=8 for control mice; n=9 for *Gch1;Lck* mice. *$P < 0.05$; **$P < 0.01$; ***$P < 0.001$ (2-tailed Student's t-test for b,d,f,i,j; 2-way ANOVA with Dunnett's comparison for g).

Figure 2. Pharmacological inhibition of the BH4 pathway ameliorates T cell mediated inflammation.

a, BH4 production in 24-hour activated control (n=5) and *Gch1*-ablated (n=5) $CD4^+$ T cells as well as wild type cells treated with SPRi3 (50μM, n=4). Experiment was repeated two independent times with similar results. Data shown as means ± s.e.m. **b,** Representative 3-day T cell proliferation histogram and quantification of stimulated wild type T cells ($CD4^+$ and $CD8^+$) treated with vehicle (n=10) or SPRi3 (50μM, n=8). Data shown as means ± s.e.m. **c,** Colitis transfer model of wild type $CD4^+$ T cells into *Rag1*$^{-/-}$ hosts treated with vehicle or SPRi3 (300mg/kg, n=8 each). Data shown as means ± s.e.m. Right panels show representative images of intestinal immune infiltration. **d,** Allergic airway inflammatory disease model in control mice treated with SPRi3 (300mg/kg, n=14) or vehicle (n=15). Data shown as means ± s.e.m. **e, f,** Proliferation of vehicle- and SPRi3-treated (50μM) naïve human (n=4 donors) peripheral blood mononuclear cell (hPBMC) **(e)** and purified effector human $CD4^+$ T cells **(f)** re-stimulated for 3 days. Data shown as means ± s.e.m. **g,** Western immunoblot of iron regulators in 24-hour activated peripheral $CD4^+$ T cells from control and *Gch1;Lck* mice. Experiment was repeated 3 independent times with similar results. **h,** Total iron content from unstimulated and 24-hour stimulated $CD4^+$ T cells from control (n=17) and *Gch1*;*Lck* (n=22) mice. Data shown as means ± s.e.m. **i,** Oxygen consumption rate (OCR) in unstimulated and 16-hour stimulated $CD4^+$ T cells from control and *Gch1;Lck* (n=6 each) mice. Data shown as means ± s.e.m. **j,** Dose-dependent reduction of ferri-cytochrome-C (CytoC-Fe^{3+}) to ferro-cytochrome-C (CytoC-Fe^{2+}) by BH4 and schematic. **k, l,** Representative oxygen uptake rate in permeabilized, 16-hour stimulated $CD4^+$ T cells from vehicle- and SPRi3-treated (50μM) wild type cells before and after the addition of reduced cytochrome-C (CytoC-Fe^{2+}) **(k)** and quantification of oxygen rate upon supplementation of CytoC-Fe^{2+} (n=4 independent experiments) **(l)**. Data shown as means ± s.e.m. *P < 0.05; **P < 0.01; ***P < 0.001 (2-tailed Student's t-test for b,d,e,f,h,I,l; 1-way ANOVA with Dunnett's comparison for a; 2-way ANOVA with Sidak's comparison for c).

Figure 3. Development of an orally available, potent small molecule SPR inhibitor to limit BH4 production.

a, Chemical structure of SPRi3 and QM385. **b,** Dose-dependent reduction in plasma BH4 levels by QM385 and respective dose-dependent increase in sepiapterin plasma levels. BQL, below quantifiable limits; <0.3ng/ml for sepiapterin. Data shown as means ± s.e.m. N=6 mice for each

condition. **c,** Representative histograms depicting 3-day proliferation of stimulated $CD4^+$ T cells with vehicle (n=4 mice) and QM385 treatment (2.5 and 5 μM, n=3 mice each) and quantitative analysis of total cell numbers**.** Data shown as means ± s.e.m. Experiment was repeated two independent times with similar results. **d,** Schematic for the house dust mite (HDM) allergy model with dose-response administration of QM385 PO twice a day for 3 consecutive days as indicated and quantification of T cells and eosinophils in bronchoalveolar lavage fluid (BALFs). Data shown as box and whisker (running from minimal to maximal values) plots for which individual data points are shown. Vehicle (n=10), 0.3mg/kg (n=5), 1mg/kg (n=4), 3mg/kg (n=6/7). Absolute numbers in the BALF are shown. *P < 0.05; **P < 0.01; ***P < 0.001; NS, not significant (One-way ANOVA with Dunnett's multiple comparisons for d,e).

Figure 4. Enhanced BH4 production results in enhanced T cell proliferation and anti-cancer immunity

a, Fold change of BH4 levels after 24-hour stimulation of $CD4^+$ T cells. Data for individual mice (n=3) as means ± s.e.m. **b,** Representative histograms after 3 days of $CD4^+$ T cell proliferation from control (n=4) and *GOE;Lck* (n=5) mice. Data are means ± s.e.m. **c,** BH4 measurements after 24 hours in activated wild type $CD4^+$ T cells treated with vehicle or sepiapterin (Sep, 5μM). Data shown for individual mice (n=5) as means ± s.e.m. **d,** Orthotopic E0071 breast cancer model in control (n=6) and *GOE;Lck* (n=7) mice. **e,** Effect of BH4 supplementation on cancer growth. BH4 (n=10 mice) and vehicle (n=9 mice) supplementation was carried out for 7 days as indicated (black line). **f,** Quantification of intratumoral effector $CD8^+$ T cells ($CD44^+CD62L^{lo}$) assayed from E0071 tumors on day 28 of vehicle (n=5) and BH4-treated (n=5) mice. Data shown as means ± s.e.m. **g,** Effect of BH4 supplementation on cancer growth in *Rag2* KO female hosts. BH4 and vehicle supplementation (n=9 mice each) was carried out for 7 days as indicated (black line). Data are means ± s.e.m., **h,** Proliferation quantification of stimulated $CD4^+$ T cells treated with kynurenine (50μM) and BH4 (10μM). Data are means ± s.e.m. N=3 samples for each condition. Experiment was repeated two independent times with similar results. **i,** Quantification of the mean fluorescent intensity (MFI) of DHE in stimulated wild type $CD4^+$ T cells treated with vehicle, kynurenine (KYN) alone (50μM) or KYN (50μM) plus BH4 (10μM) for 20 hours. Data are means ± s.e.m. N=3

samples for each condition. Experiment was repeated two independent times with similar results. *P < 0.05; **P < 0.01; ***P < 0.001; ****P < 0.0001 (2-tailed Student's t-test for a,b,c,f; 2-way ANOVA with Sidak's comparison for d,g; 1-way ANOVA with Tukey's comparison for h,1).

Materials and Methods

Mice. Mice expressing eGFP under the *Gch1* promoter were used to label cells that upregulate *Gch1* after T cell activation. Mice with a *Cre*-dependent *GCH1*-HA overexpression cassette to induce BH4 overproduction and *Gch1* floxed mice prevented BH4 production have been previously reported[1,5]. For both gain- and loss-of-function experiments, we bred *GCH1*-HA and *Gch1* floxed mice to the T cell-specific lines *LCK-Cre*[28], *CD4-Cre*[29], *RORgammact-Cre* or the ubiquitous tamoxifen-inducible *Rosa26-Cre*ERT2[30] animals and also to the B cell-specific line, *MB1-Cre*. All animal experiments were approved by the Austrian Animal Care and Use Committee.

Compounds. Sepiapterin (Sep, 11.225), tetrahydrobiopterin (BH4, 11.212) were purchased from Schircks Labs, Switzerland. For *in vitro* use, both sepiapterin and BH4 were dissolved in DMSO to a stock concentration of 10mM. SPRi3 has been previously developed and was used as instructed[1]. For T cell assays, sepiapterin was used at a concentration of 5μM, BH4 at a concentration of 10μM and SPRi3 at a concentration of 50μM unless otherwise stated in the figure legends. For *in vivo* use, BH4 was reconstituted in sterile saline under argon gas. Kynurenine (# K8625) and NAC (# A9165) were purchased from Sigma.

Determination of BH4 levels. BH4 (tetrahydrobiopterin), and oxidized biopterins (BH2 and biopterin,) were determined by high-performance liquid chromatography (HPLC) followed by electrochemical and fluorescent detection, respectively, following an established protocol[31]. Cell pellets were freeze–thawed in ice-cold resuspension buffer (50mM phosphate-buffered saline, 1 mM dithioerythriol, 1 mM EDTA, pH 7.4). After centrifugation at 13,200 rpm for 10 min at 4°C, supernatant was removed and ice-cold acid precipitation buffer (1 M phosphoric acid, 2 M trichloroacetic acid, 1 mM dithioerythritol) added. Following centrifugation at 13,200 rpm for 10 min at 4°C, the supernatant was removed and injected onto the HPLC system. Quantification of BH4 and oxidized biopterins was obtained by comparison with external standards and normalized to protein concentration, determined by the BCA protein assay (Pierce).

Determination of sepiapterin levels by HPLC. Supernatant samples were precipitated by the addition of 1 volume (1:1, v/v) of TCA 5% + DTE 6.5mM. Afterwards, samples were centrifuged (10,000 x g for 10 min at 4ºC) and 20ul analyzed. HPLC analysis of sepiapterin was done using a Beckman System Gold (Beckman Instruments, Inc., Fullerton, CA USA) by using a Waters Atlantis dC-18, 5 μm RP column (4.6 × 250 mm; temperature 35 °C), with a flow rate set at 0.5 mL/min and isocratic elution of mobile phase (92% phosphate buffer (15mM); 8% acetonitrile

(90%), pH 6.4). Identification and quantification of sepiapterin was done using a multi-wavelength fluorescence detector (ex. 425 nm, em. 530 nm, module 2475, Waters, Milford, USA) and expressed as nM of sepiapterin.

Lymphocyte proliferation. T cells were purified from spleens and lymph nodes of mice using microbeads ($CD4^+$; $CD8^+$, naïve $CD4^+$, Miltenyi Biotec). 96 U-shaped plates were coated with anti-CD3 (4μg/ml, Biolegend) with/without anti-CD28 (2μg/ml, Biolegend) at the indicated concentrations unless otherwise stated in the figure legends in PBS for 3 hours at 37°C. T cells were then plated at 10^5 cells/well in IMDM+PenStrep+Lgly+10% FCS. Beta-mercaptoethanol was omitted. PMA (50ng/ml) and ionomycin (50ng/ml) were also used to stimulate purified T cells for 24 hours. Purified and activated T cells were cultured for 24 hours and expression of activation markers (CD62L, CD25, CD44, CD69) were analyzed using flow cytometry and the supernatant was collected in which IL-2 and IFNγ concentrations were measured using ELISA kits (Biolegend). Purified T cells were also stained with the Cell Violet Trace Proliferation Kit (Invitrogen), cultured for 3 days and proliferation was assayed by flow cytometry on viable cells (DAPI-negative). In addition, purified T cells were cultured with purified splenic dendritic cells and soluble anti-CD3 antibody (1μg/ml) for three days. For iNOS expression, purified CD4+ T cells were stimulated and assayed fixed and permeabilized at the various time points and stained for iNOS levels. B cells were purified using microbeads ($CD19^+$; Miltenyi Biotec) from the spleen, loaded with cell tracer, stimulated with LPS (1μg/ml) and analyzed for proliferation as described above. For class switch recombination experiment, $CD43^-$ B cells were isolated from spleens by MACS (Miltenyi Biotec) and stimulated for 5 days with LPS (20 μg/ml) to induce switching to IgG3. Percentages of switched B lymphocytes were assessed by flow cytometry

EdU staining. The cell cycle status of T cells was assessed using the Click-iT® EdU Flow Cytometry Cell Proliferation Assay (Invitrogen). Briefly, purified $CD4^+$ T cells were activated with anti-CD3 (4μg/ml) and anti-CD28 (2μg/ml) as described above. EdU was pulsed into the wells for 4 hours after 16hrs of stimulation. The cells were prepared and stained with EdU as per the manufacturer's instructions.

Mitochondrial respiration and metabolomics. Mitochondrial respiratory parameters were measured with high-resolution respirometry (Oxygraph-2k, Oroboros Instruments, Innsbruck, Austria)[32]. Routine respiration was measured by incubating cells in a buffer containing 110 mM sucrose, 60 mM K-lactobionate, 20 mM K-HEPES, 10 mM KH_2PO_4, 3 mM $MgCl_2$, 0.5 mM EGTA and 1 g/L fatty acid-free bovine serum albumin at 37°C (pH 7.2). Total capacity was induced by titration of carbonyl cyanide-4-(trifluoromethoxy)phenylhydrazone (Sigma Aldrich) in steps of 0.5 μM. To assess Complex I- and Complex II-linked respiration, cells were permeabilized with digitonin [8 μM]. Complex I-linked State 3 respiration was induced by addition of 5 mM glutamate/5 mM malate and 1mM adenosine diphosphate (ADP). Complex II-linked State 3 respiration was induced with 10mM succinate after addition of the Complex I inhibitor rotenone (1ng/mL). To restore respiratory function in activated CD4+ T cells, cells were permeabilized with digitonin [12 μM] and exogenous reduced cytochrome c (2.5 μM; Abcam,

b140219) was added. Respiration rates were obtained by calculating the negative time derivative of the measured oxygen concentration. Oxygen consumption rates were measured using Seahorse technology. To measure ATP, purified T cells were either left unstimulated or stimulated with plate-bound anti-CD3 (4μg/ml) and anti-CD28 (2μg/ml) for the times indicted in the figure. ATP was measured using the CellTiter-Glo® Luminescent Cell Viability Assay (Promega). To determine ROS levels, purified T cells were activated with anti-CD3 plate-bound anti-CD3 (4μg/ml) and anti-CD28 (2μg/ml) for 10 hours. Cells were washed once with HBSS and stained in 10μM DHE (Invitrogen) for 30 mins at 37^{o}C. Cells were washed 2X with HBSS and assayed by flow cytometry. Profiling of biogenic amines by hydrophilic interaction liquid chromatography (HILIC-QTOF) mass spectrometry was performed on cell pellets and supernatants from unstimulated and TCR-stimulated purified T cells by the West Coast Metabolomics Center (UC Davis). For NO_2- measurements we used the Griess reagent system (TB229, Promega). Purified T cells were stimulated with anti-CD3 and anti-CD28 antibodies as described above and the supernatant was collected at various timepoints for nitrite measurements. Peritoneal macrophages stimulated with LPS (100ng/ml) for 24 hours were used as a positive control.

Flow cytometry. Antibody labeling of cells was carried out in FACS staining buffer (PBS supplemented with 2% FCS and 2 mM EDTA) on ice for 30 min after blocking Fc receptors. See Supplemental Table 4 for a list of antibodies used in this study. Cells were recorded on an LSR II flow cytometer (BD Biosciences), and data were analyzed using FlowJo v10.0.6 software (Tree Star). Absolute splenocyte and thymus numbers were determined by counting total cells with a CASY1 counter and subsequent calculation of T cell and B cell numbers based on ratios from FACS experiments.

Protein blotting. Protein blotting was carried out using standard protocols. Blots were blocked for 1 hour with 5% BSA in TBST (1× TBS and 0.1% Tween-20) and were then incubated overnight at 4°C with primary antibodies (See Supplemental Table 4), diluted in 5% BSA in TBST (1:1,000 dilution). Blots were washed three times in TBST for 15 min and were then incubated with HRP-conjugated secondary antibodies (1:2,500 dilution; GE Healthcare, NA9340V) for 45 min at room temperature, washed three times in TBST for 15 min and visualized using enhanced chemiluminescence (ECL Plus, Pierce, 1896327).

OP9-DL1 co-cultures. OP9 bone marrow stromal cells expressing the Notch ligand DL-1 (OP9-DL1; kindly provided by Juan Carlos Zúñiga-Pflücker; University of Toronto) were maintained as described previously[33]. 10^4 OP9-DL1 were plated per well in 48 well plates 4-12 hours before the start of thymocyte cultures. DN3a thymocytes were sorted as TCRβ^{-}TCRγδ^{-}CD4^{-}CD8a^{-} CD28^{-}CD25^{hi}CD44$^{-/lo}$ cells using a BD FACS Aria sorter. CellTrace Violet labeling of the sorted cells was performed in 1 μM CellTrace Violet solution in PBS containing 0.1% BSA for 7 min at 37^{o}C. Cells were washed with medium containing 20% FCS. Thymocytes were then plated on the OP9-DL1 monolayers in the presence of 5 ng/ml Flt3L. Co-cultures were performed in αMEM supplemented with 10 mM HEPES (pH 7.5), 1 mM sodium pyruvate, 100 U/ml penicillin, 0.1 mg/ml streptomycin, and 20% heat inactivated FBS.

Adoptive transfer model of colitis. $5x10^5$ MACS-purified naive $CD4^+CD62L^+$ T cells from control and *GCH1;Lck* mice were injected i.p. into 6- to 8 weeks old *Rag1*$^{-/-}$ mice. After the cell transfer, *Rag1*$^{-/-}$ recipients were weighed weekly and monitored by mini-endoscopy. For monitoring of colitis activity, a high-resolution video endoscopic system (Karl Storz) was used. To determine colitis activity, mice were anesthetized by injecting a mixture of ketamine (Ketavest 100mg/ml, Pfizer) and xylazine (Rompun 2%, Bayer Healthcare) i.p. and monitored by mini-endoscopy at the indicated time-points. Endoscopic scoring of five parameters (translucency, granularity, fibrin, vascularity and stool) was performed (Supplemental Table 5)[34]. For histological analysis, colonic cross sections were stained with H&E. Immunofluorescence of cryo-sections was performed using the TSA Cy3 system (PerkinElmer) and a fluorescence microscope (IX70; Olympus) using primary antibodies against F4/80, MPO, CD3, CD4 and CD11c. In brief, cryo-sections were fixed in ice-cold acetone for 10 minutes followed by sequential incubation with methanol, avidin/biotin (Vector Laboratories), and protein blocking reagent (DAKO) to eliminate unspecific background staining. Slides were then incubated overnight with primary antibodies specific for the respective antigen. Subsequently, the slides were incubated for 30 minutes at room temperature with biotinylated secondary antibodies (Dianova). All samples were finally treated with streptavidin-horseradish peroxidase and stained with Tyramide (Cy3) according to the manufacturer's instructions (Perkin Elmer). Before examination, nuclei were counterstained with Hoechst 3342 (Invitrogen). For Treg transfer experiments[35], 500,000 T conventional cell ($CD4^+CD25^-CD45RB^{hi}$) and 500,000 Treg cells ($CD4^+CD25^+CD45RB^{lo}$) were transferred i.p. into *Rag2* KO hosts. For *GOE;CD4* $CD4^+$ T cell transfer, 150,000 cells were transferred. Body weights were monitored over the course of the experiment[35]

OVA immunization and airway hyperresponsiveness. For OVA immunization study, immunization was performed using 100µg OVA per mouse in 200µL Alum intraperitoneally (i.p.). Blood was collected from the tail vein 14 days after injection to check IgG and IgM titers. 3 weeks later a further i.p. injection was carried out and again blood collected two weeks later to measure the re-challenge responses. For measurements of lung function, deeply anesthetized mice (pentobarbital (60 mg/kg) underwent a tracheotomy with a 20G sterile catheter. A computer-based analysis of airway hyperresponsiveness was then performed using a Flexivent (SCIREQ) apparatus[10]. Mice were ventilated at a tidal volume of 9 ml/kg with a frequency of 150 bpm; positive end-expiratory pressure was set at 2 cm H2O. Lung resistance and elastance of the respiratory system was determined in response to in-line aerosolized methacholine challenges (0, 1, 3, 10, 30, 100 mg/ml). Methacholine was dissolved in sterile PBS. The mean elastance and resistance of 10 measurements by doses was calculated. For bronchoalveolar lavage (BAL) on day 21, mice were anesthetized following an intraperitoneal injection of urethane (200 µl i.p., 35%) and a 20G sterile catheter inserted longitudinally into the trachea. 2 ml of ice cold PBS containing protease inhibitors (Roche) was injected into the lung, harvested and stored on ice. BAL fluid underwent a 400g centrifugation (15 min; 4^{o}C), the supernatant was discarded and cells resuspended in 200 µl[10]. Bronchoalveolar lavage fluid (BALF) cells were resuspended in FACS buffer (PBS, 2% FCS, EDTA), and incubated with Fc block (0.5 mg/ml, 10 min; BD Biosciences). Cells were then stained with monoclonal antibodies (FITC anti-mouse CD45, BD

Biosciences, cat no: 553079, PE anti-mouse Syglec-F, BD Biosciences, cat no: 552126; APC anti-mouse GR-1, eBiosciences, cat no: 17-5931-81; PE-Cy7 anti-mouse CD3ε, cat no: 25-0031-81; PerCP anti-mouse F4/80, BioLegend, cat no: 123125; 45 min, 4^{o}C on ice) before data acquisition on a FACS Canto II (BD Biosciences). A leukocyte differential count was performed during flow cytometry analysis of cells expressing the common leukocyte antigen CD45 (BD Pharmigen; cat no: 553079). Specific cell populations were identified as follows: macrophages as F4/80^{Hi}-Ly6g^{Neg}, eosinophils as F4/80^{Int}-Ly6g^{Lo}-SiglecF^{Hi}, neutrophils as F4/80^{Lo}-Ly6g^{Hi}-SiglecF^{Neg}, and T lymphocytes as F4/80^{Neg}-Ly6g^{Neg}-CD3^{Pos}. Total BAL cell counts were performed using a standard hemocytometer, with absolute cell numbers calculated as total BAL cell number multiplied by the percentage of cell subpopulation as determined by FACS[10].

House Dust Mite (HDM) allergy model. For house dust mite induced lung inflammation, C57Bl/6 animals (Female, 6-12 weeks old) were sensitized for two consecutive days with 25ug House Dust Mite Extract (HDM) (*D. pteronyssinus*, Greer laboratories, XPB82D382.5) intranasally. Six days after the last sensitizing dose, mice were challenged with 12.5ug of HDM for five consecutive days, with 3mg/kg QM-760 (in 1% tween 80 and 0.5% sodium carboxymethyl cellulose, Sigma-Aldrich, St. Louis, MO) administered by oral gavage, twice daily on days 3-5 during the challenge phase. Bronchoalveolar lavage fluid (BALF) was removed and analyzed for the following immune cell subsets three days after the last challenge:T-cells: CD45^{+}, Thy1^{+}, CD3^{+}, CD11b^{-}, Siglec-F^{-}, Ly6C/G^{-}**;** Eosinophils: CD45^{+}, Thy1^{+}, CD11b^{+}, Siglec-F^{+}, CD3^{-}, Ly6C/G^{-}

Skin hypersensitivity. The skin contact hypersensitivity model was performed as previously described[11]. Briefly, for the induction of contact hypersensitivity, mice were sensitized on day 0 by applying 100 µl of 7% 2,4,6-trinitrochlorobenzene (TNCB-Sigma)/acetone or acetone alone as vehicle control on the shaved abdomen. On day 5 mice were challenged on the dorsum of both ears with 20 µl of 1% TNCB/acetone. Ear thickness was measured immediately before and 24 hours after the challenge.

Experimental autoimmune encephalitis (EAE). EAE was induced in control and *Gch1;Lck* mice by immunization with an emulsion of 100µg MOG$_{35-55}$ in complete Freund's adjuvant (CFA), supplemented with 5mg/ml Mycobacterium tuberculosis (Difco). 100 µL MOG/CFA was injected subcutaneously above the inguinal lymph node on both sides of the mouse. 200 µL pertussis toxin/PBS (50ng/µL-List Biological Labs) was injected intraperitoneally per mouse on day 0 and day 1. Scoring for EAE was performed as previously described over the course of 45days[36].

Orthotopic cancer models. E0771 cells were orthotopically injected into syngeneic control and *GOE;Lck* mice as previously described[21]. In brief, cells were harvested for injection into mice by trypsin digestion for 5 minutes, washed in Hank's Balanced Salt Solution, counted, diluted in this salt solution and orthotopically injected into the fat pad of the fourth mammary gland (2.5x10^{5} cells/200µL/mouse). BH4 administration was delivered i.p. (100mg/kg) after tumors were

palpable (day 10) and treatment was continued for 7 days. Tumors were measured using digital calipers; the size of the tumor was expressed as length (mm) x width (mm) x height (mm) = tumor size (mm^3). The tumor cell line, TC-1, was derived from primary lung epithelial cells of C57BL/6 mice. The cells were immortalized with the amphotropic retrovirus vector LXSN16E6E7 and subsequently transformed with the pVEJB plasmid expressing the activated human c-Ha-ras oncogene[37]. This cell line was treated and injected into wild type and *Rag2*$^{-/-}$ mice as described above. After collagenase/dispase digestion of the tumors, intratunoral effector $CD4^+$ and $CD8^+$ T cells were charaterised by flow cytometry ($CD62L^{lo}$, $CD44^{hi}$).

Microarray analysis. Purified $CD4^+$ T cells from control and *Gch1;Lck* mice were stimulated with plate bound anti-CD3 (4μg/ml) and anti-CD28 (2μg/ml) for 16 hours and total RNA was extracted by sequential Qiazol extraction and purification through the RNeasy micro kit with on column genomic DNA digestion (Qiagen). RNA quality was determined by an Agilent 2100 Bioanalyzer using the RNA Pico Chip (Agilent). RNA was amplified into cDNA using the Ambion wild-type expression kit for whole transcript expression arrays, with Poly-A controls from the Affymetrix Genechip Eukaryotic Poly-A RNA control kit. Images from Agilent arrays were processed by Agilent Feature Extraction Software 10.7.3.1. Raw intensity data were processed in R v3.4.0 using limma v3.34.3 applying normexp background calculation, lowess within-array and Aquantile between-array normalization methods. The normalized values were used to calculate log2 transformed Cy5/Cy3 ratios. Differentially expression analysis was performed by fitting a linear model to the normalized data and computing empirical Bayes test statistics in limma accommodating a mean-variance trend[38]. False discovery rate was controlled by Benjamini-Hochberg adjustment. The data discussed in this publication have been deposited in NCBI's Gene Expression Omnibus[39] and are accessible through GEO Series accession number GSE108101 (https://www.ncbi.nlm.nih.gov/geo/query/acc.cgi?acc=GSE108101).

Ferric/Ferrous reduction. The enzymatic activity of BH4 was assayed as previously described[40]. The enzymatic conversion of qBH2 to BH4 was followed by the reduction of Ferricytochrome-c (FICC) to Ferrocytochrome-c (FOCC) by BH4. FICC reduction was determined by reading the increasing FOCC absorbance signal at 550nm. The experiment was run for 40 minutes at pH 7.4 and recorded at 10 seconds intervals in 200μl buffer containing 50μM FICC, 1μM 6-methyltetrahydropterin (6MPH4), 20nM DHPR, 50μM NADH and selected inhibitors. A control lacking DHPR was ran in parallel to assess the rate of non-enzymatic reduction of qBH2 by NADH. The extinction coefficient used for FOCC and NADH are respectively 29500 (reduced, 550nm, H_2O) and 6220 (340nm, H_2O) [$L \cdot mol^{-1} \cdot cm^{-1}$]. Generally, 50μM of FOCC and FICC in buffer were measured in isolated wells to assess completion of the reaction.

Iron Measurements. Total iron content was measured as previously described[41]. Briefly, intracellular iron measurements were carried out by using a PerkinElmer Analyst 800 equipped with a transversely heated graphite atomizer (THGA). A Zeeman-effect background correction was realized by a 0.8 T magnetic field, oriented longitudinally with respect to the optical path. A PerkinElmer Lumina single-element iron hollow cathode lamp was driven at a constant current of

30 mA after proper equilibration (i.e., ≥20 min). For the absorption measurements, the 248.3-nm line (spectral bandwidth 0.7 nm) was chosen. FACS-purified naïve $CD4^+$ T cells from control and *Gch1;Lck* mice were left untreated or stimulated (anti-CD3 and anti-CD28) for 12 hours. The cells were then pelleted and frozen at -80°C. Next, the samples were suspended in 200 µl of a 0.1% (v/v) solution of nitric acid (Rotipuran Supra, 69%, Carl Roth GmbH, Karlsruhe, Germany) in high-purity water (Milli-Q, Merck-Millipore, Darmstadt, Germany) by extended periods (i.e., ≥30 min) of vortexing and ultrasonication at 30-40 kHz. After an initial estimation of the sample's iron quantity, a five-point linear calibration was established in the range between 0 (i.e., <0.004 µM) and 0.106 µM. The calibration standards were prepared by diluting a 0.1 M standard stock solution of $(NH_4)_2Fe(SO_4)_2$ (Merck-Millipore, Darmstadt, Germany) with a 0.1% (v/v) aqueous solution of nitric acid (vide supra). The absence of detectable iron (i.e., <0.004 µM) in the dilution agent, as well as in the sample cups, and the glassware was verified throughout the analyses. A linear fit of the 15 data points (k = 0.978, d = 0.006 µM) yielded a coefficient of determination of 0.992. Samples with iron concentrations exceeding the calibration range (i.e., ≥0.106 µM) were diluted appropriately. The blank solution, the calibration standards, and the samples were supplied to the atomizer in randomized fashion as triplicates, using a PerkinElmer AS-800 autosampler with an injection volume of 20 µl. The solvent was evaporated by a slow temperature gradient to 130 °C, ashing took place at a maximum temperature of 1,000 °C, and the atomization profile was read at 2,000 °C. The graphite tube, which was protected against oxidation by high-purity argon (99.999%, Messer Austria GmbH, Gumpoldskirchen, Austria), was cleaned out after each analysis at 2,450 °C. The integrity of each analysis was verified by a visual inspection of the respective time-dependent atomization profile.

Human T cell proliferation assays. Proliferation of peripheral blood mononuclear cells (PBMCs), obtained from healthy blood donors, was assessed following cell exposure to Dynabeads Human T Activator CD3/CD28 (bead/cell ratio: 1/2) and IL2 (30 IU/ml), in the absence or presence of vehicle (DMSO) or SPRi3 (50µM). PBMCs were resuspended in RPMI 1640 medium supplemented with 2mM L-glutamine, 100U/ml penicillin, 100 mg/ml streptomycin, 1% non-essential amino acids and 10% FBS, seeded at $2.5x10^5$/well and cultured for 5 days. For the last 18 hours of culture, cells were pulsed with 0.25 mCi/well ^{3}H-thymidine. Incorporated thymidine was measured by liquid scintillation spectroscopy. In addition, we also determined the proliferation of alloreactive human T cells. PBMCs from a healthy donor were stimulated with M21 tumor cells. Alloreactive T cells-based on MHC mismatch were cultured for 2 weeks. Afterwards, effector $CD4^+$ T cells were sorted (regulatory T cells excluded), CFSE-labelled, and stimulated with anti-CD3 and anti-CD28 for 5 days with either DMSO or SPRi3 (50µM) supplementation. For QM385 studies, PBMCs from to donors were stimulated with plate-bound anti-CD3 and anti-CD28 (1µg/ml each). On Day 3 of stimulation, the number of $CD4^+$ T cells were counted by FACS. PBMCs were isolated from healthy subjects (Blood Donor Center at Children's Hospital Boston, MA). Human studies received IRB approval (2011P000202) from Beth Israel Deaconess Medical Center Ethics Committee and written consent was obtained from all study participants prior to inclusion in the study.

QM385 compound analysis. SNAP-based competition time-resolved-FRET (TR-FRET) assay. Purified SNAP-SPR and Sulfasalazine-SNAP-mEGFP were labeled with 2-fold excess of

benzylguanine-Terbium cryptate conjugate (K2-benzylamide-BG, Cisbio) or benzylguanine-sulfasalazine (BG-SSZ) respectively and purified with NAP5 columns (GE healthcare) to remove excess of labeling reagents. Final reaction mixture contained 2.0 nM Tb-SNAP-SPR, 70 nM SSZ-SNAP-mEGFP, 10 μM NADPH, 10 μM NADP+ in buffer A (50 mM HEPES-NaOH pH7.4, 0.15 M NaCl, 0.5 μg/μl BSA, 0.05% Triton X-100, 1 mM DTT). Signal was measured after 3 h of incubation with varying concentrations of QM385 using Infinite F500 (TECAN). Excitation wavelength was 320 nm, emission wavelengths were 485 nm and 520 nm respectively. For BH4 measurements, 50,000 human PBMCs were plated in 96-well plates coated with 1ug/ml human anti-CD3. Cells were incubated with 1ug/ml soluble human anti-CD28 for 48hours with varying doses of QM385 as indicated in the figure. Cell were then harvested for LC-MS BH4 measurements. Similar experiments were performed on anti-CD3/28 activated mouse splenocytes.

Plasma levels of QM385. To formulate 10mg/kg of QM385 for oral administration, 6.312 mL of 1%Tween 80 + 0.5% HPMC in 50mM carbonate buffer (pH=9.0) were added into a tube containing 7,98 mg of the compound, then vortexed t for 1-2 min and sonicated for 30-35 min**.** Solutions were prepared just prior to use. The IV dosing solution was prepared in 10%DMAC, 10% Solutol HS15, 80%(10%HP-β-CD) in saline(w/v). Approximately 100 μL of blood sample was collected via tail vein into EDTA-2K tubes. The blood samples were maintained in wet ice first and centrifuged to obtain plasma (2000g, 4℃, 5 min) within 15 minutes post sampling. An aliquot of 30 μL serum sample was added with 100 μL ACN containing 10 ng/mL IS (Dexamethasone). The mixture was vortexed for 2 min and centrifuged at 14000 rpm for 5 min. An aliquot of 10 μL supernatant was injected for LC-MS/MS analysis. A calibration curve 0.100-1000 ng/mL for QM385 in C57BL/6 mouse diluted blood was also prepared.

Statistical analyses. All values are expressed as means +/- s.e.m. Details of the statistical tests used are stated in the figure legends. Briefly, Student's t-test was used to compare between two groups. One-way ANOVA followed by Dunnett's post-hoc test for multiple comparisons was used for analysis between multiple groups. 2-way ANOVA was used to compare two groups over time. In all tests $P \leq 0.05$ was considered significant.

Data availability. Microarray dataset is accessible through GEO Series accession number GSE108101. All other datasets generated during and/or analysed during the current study are available from the corresponding authors upon reasonable request

SUPPLEMENTARY REFERENCES

28. Hennet, T., Hagen, F. K., Tabak, L. a & Marth, J. D. T-cell-specific deletion of a polypeptide N-acetylgalactosaminyl-transferase gene by site-directed recombination. *Proc. Natl. Acad. Sci. U. S. A.* **92,** 12070–4 (1995).

29. Sawada, S., Scarborough, J. D., Killeen, N. & Littman, D. R. A lineage-specific transcriptional silencer regulates CD4 gene expression during T lymphocyte development. *Cell* **77,** 917–929 (1994).

30. Ventura, A. *et al.* Restoration of p53 function leads to tumour regression in vivo. *Nature* **445,** 661–665 (2007).

31. Crabtree, M. J. *et al.* Quantitative regulation of intracellular endothelial nitric-oxide synthase (eNOS) coupling by both tetrahydrobiopterin-eNOS stoichiometry and biopterin redox status insights from cells with TET-regulated GTP cyclohydrolasei expression. *J. Biol. Chem.* **284,** 1136–1144 (2009).

32. Banerjee, A. *et al.* Cellular and Site-Specific Mitochondrial Characterization of Vital Human Amniotic Membrane. *Cell Transplant.* **27,** 3–11 (2018).

33. Schmitt, T. M. & Zúñiga-Pflücker, J. C. Induction of T cell development from hematopoietic progenitor cells by delta-like-1 in vitro. *Immunity* **17,** 749–756 (2002).

34. Becker, C. *et al.* In vivo imaging of colitis and colon cancer development in mice using high resolution chromoendoscopy. *Gut* **54,** 950–954 (2005).

35. Collison, L. W. & Vignali, D. A. A. In vitro Treg suppression assays. *Methods Mol. Biol.* **707,** 21–37 (2011).

36. Boivin, N., Baillargeon, J., Doss, P. M. I. A., Roy, A. P. & Rangachari, M. Interferon-?? suppresses murine Th1 cell function in the absence of antigen-presenting cells. *PLoS One* **10,** (2015).

37. Lin, K. Y. *et al.* Treatment of established tumors with a novel vaccine that enhances major histocompatibility class II presentation of tumor antigen. *Cancer Res.* **56,** 21–26 (1996).

38. Smyth, G. K. Linear Models and Empirical Bayes Methods for Assessing Differential Expression in Microarray Experiments. *Stat. Appl. Genet. Mol. Biol.* **3,** 1–25 (2004).

39. Edgar, R. Gene Expression Omnibus: NCBI gene expression and hybridization array data repository. *Nucleic Acids Res.* **30,** 207–210 (2002).

40. Arai, N., Narisawa, K., Hayakawa, H. & Tada, K. Hyperphenylalaninemia due to dihydropteridine reductase deficiency: diagnosis by enzyme assays on dried blood spots. *Pediatrics* **70,** 426–30 (1982).

41. Theurl, I. *et al.* On-demand erythrocyte disposal and iron recycling requires transient macrophages in the liver. *Nat. Med.* **22,** 945–951 (2016).

Legends to Extended Data Figures

Extended Data Figure 1. Upregulation of *Gch1* and BH4 in activated T cells

a, Percentage of GFP^+ cells from 24 hour-PMA/ionomycin (50ng/ml each) stimulated purified *Gch1-Gfp* $CD4^+$ T cells. Data are shown as means ± s.e.m. Data from n=3 samples are indicated. Experiment was repeated 2 independent times. ***P < 0.001 (2-tailed, Student's t-test). **b, c,** Representative *Gch1-Gfp* expression in 16 hour-activated ($CD62L^{lo}$) $CD4^+$ T cells after anti-CD3/CD28 stimulation **(b)** and representative dose-response of anti-CD3/CD28 stimulation of purified $CD4^+$ *Gch1-Gfp* T cells for 24 hours **(c)**. Experiment was repeated two independent times with similar results. **d,** Cell numbers of various immune populations in the thymus (left panel) and spleen (right panel) from control (n=3) and *Gch1;Lck* (n=3) 8-week-old mice. Data from individual mice are shown as means ± s.e.m. NS, not significant (2-tailed, Student's t-test). **e, f,** $CD4^+$ **(e)** and $CD8^+$ **(f)** T cell proliferation after 3 days of anti-CD3/28 stimulation from control and *Gch1;Lck* mice. **g,** Representative histogram depicting the proliferation of DN3a thymocytes from control and *Gch1;Lck* mice cultured on OP9-Dl1 stromal cells for 5 days. Experiment was repeat two independent times with similar results. **h,i,** Representative FACS blot depicting the differentiation of DN3a thymocytes from control and *Gch1;Lck* mice cultured on OP9-Dl1 stromal cells for 5 days into $CD4^+$ and $CD8^+$ T cells **(h)** and quantification of the differentiated cell types from n=3 animals **(i)**. Data from individual mice are shown as means ± s.e.m. NS, not significant (2-tailed, Student's t-test).

Extended Data Figure 2. Normal T cell development and B cell biology in the absence of *Gch1*

a, Thymocyte cell death induced by various stimuli over 24 hours. Anti-CD3 (0.5 and 5 μg/ml), Fas ligand (0.2 and 2 μg/ml), dexamethasone (Dex, 0.1 and 0.5 μg/ml) and γ-irradiation (1 Gray(Gy)). Data are shown as means ± s.e.m. n=3 for each genotype. NS, not significant (2-tailed, Student's t-test). **b,** Death by neglect of purified $CD4^+$ T cells cultured without stimulation for up to 56 hours. Data are shown as means ± s.e.m. n=3 for each genotype. NS, not significant (2-tailed, Student's t-test). **c, d,** $CD4^+$ T cell proliferation after 3 days of anti-CD3/28 stimulation from control and *Gch1;RORc* mice. Panels show representative FACS proliferation traces **(c)** and representative dose response **(d).** Experiments were repeated independently >6 time showing similar results. **e,** Representative FACS plots from spleens of control and *Gch1;MB1* mice depicting B cell populations. Experiment was repeated two independent times with similar results. **f, g,** Representative FACS histogram depicting LPS (1μg/ml)-stimulated B cell proliferation from control and *Gch1;MB1* mice after 3 days **(f)** as well as wild type B cells treated with vehicle (DMSO) or SPRi3 (50μM) **(g)**. Shaded grey peaks represents unstimulated cells. FACS plots are representative of two independent experiments showing similar results. n=3 mice per group. **h,** Class switch recombination. FACS analysis of splenic $CD43^-$ B cells from control and *Gch1;MB1* mice stimulated with LPS (20μg/ml) for 5

days inducing class switch recombination to IgG3. FACS plots are representative of two independent experiments showing similar results.

Extended Data Figure 3. Treg cell development and function in *Gch1*-ablated mice

a, b, Representative FACS plot depicting $CD4^+FoxP3^+$ Treg cells **(a)** and quantification of Treg proportions as well as absolute numbers in the spleen **(b)** of control and *Gch1;RORc* (n=6 each) mice. Data are shown as means ± s.e.m. *P < 0.05; **P < 0.01; ***P < 0.001; NS, not significant (2-tailed, Student's t-test). **c, d,** *In vitro* Treg suppression assay whereby naïve, wild type $CD4^+$ T cells were activated in the presence of varying ratios of Treg cells from control and *Gch1;RORc* mice for 4 days. Representative histogram showing suppressive capacity of control and *Gch1;RORc* Treg cells **(c)** and quantification of proliferation with various ratios of Treg cells **(d)**. N=4 samples. Data are shown as means ± s.e.m. *P < 0.05; **P < 0.01; NS, not significant (2-tailed, Student's t-test with multiple comparisons). **e,** Naive $CD4^+$ transfer colitis model with co-transfer of FACS-purified Treg cells from control (n=4) and *Gch1;RORc* (n=4) mice. Control Tconv (n=16 mice) with no Treg co-transfer were used. Changes to initial body weight (BW) were scored over 5 weeks. Data are shown as means ± s.e.m. *P < 0.05; ***P < 0.001; NS, not significant (Two-way ANOVA with Tukey's multiple comparison test). **f,** Total numbers of $CD4^+$ splenic T cells at 2 weeks post-transfer in mice (n=3) transferred with naïve CD4+ cells only (no Tregs) and mice transferred with Tregs from control and Gch1-ablated (*Gch1;RORc*) mice. Data are shown as means ± s.e.m. ***P < 0.001; ****P < 0.0001; NS, not significant (One-way ANOVA with Dunnett's multiple comparison test). **g,** Transfer colitis model of intestinal autoimmunity. Body weight changes relative to initial weight between mice transferred with naïve CD4+ T cells from control and *Gch1;Lck* mice (n=10 each). Data are shown as means ± s.e.m. NS, not significant (Two-way ANOVA with Sidak's multiple comparisons). **h, i,** Proportion of $CD4^+$ T cells in the draining mesenteric lymph nodes **(h)** on week 4 and intracellular cytokine profiles (IFNγ and IL-17) from transferred control and *Gch1;Lck* cells **(i).** Data are shown as means ± s.e.m. N=10 for each genotype for (h) and n=5 for each genotype for (i). ***P < 0.001; NS, not significant (2-tailed, Student's t-test).

Extended Data Figure 4. Blockage of GCH1/BH4 abrogates T cell-mediated autoimmunity.

a, Ova-immunisation of control and *Gch1;Lck* mice. T cell-dependent IgG responses and T cell-independent IgM responses are shown two weeks after OVA immunization (100μg OVA in 200μg alum) as well as two weeks after re-challenge. n=5 for control mice; n=6 for *Gch1;Lck* mice. Data are shown as means ± s.e.m. *P < 0.05; **P < 0.01; ***P < 0.001; NS, not significant (2-tailed, Student's t-test with multiple comparisons). **b, c,** EAE model of CNS autoimmunity. Data are shown as means ± s.e.m. **b,** EAE scores of control and *Gch1;Lck* mice. n = 6 for each genotype. ****P < 0.0001 (linear regression analysis was performed on the slope of each curve). **c,** Mean maximal EAE severity in control and littermate *Gch1;Lck* mice. *P <

0.05 (Mann-Whitney test). **d,** Schematic representation of the de novo, salvage and recycling arms of the BH4 pathway. Dotted arrow indicates non-enzymatic reactions while solid arrows indicate enzymatic reactions. *GTP*, guanosine triphosphate; *PTPS*, 6-Pyruvoyl tetrahydropterin synthase; *DHFR*, dihydrofolate reductase; *SPR*, sepiapterin reductase; *QDPR*, quinoid dihydropteridine reductase; *PCDB*, pterin-4alpha-carbinolamine dehydratase. **e,** Representative FACS plots depicting activation marker profiles of purified wild type control $CD4^+$ T cells left unstimulated or anti-CD3/28-stimualted for 16 hours and treated with vehicle (DMSO), SPRi3 (50μM) or Sep (5μM). Experiment was repeated two independent times with similar results. **f,** Cell survival as defined by $DAPI^-AnnexinV^-$ cells of purified $CD4^+$ T cells stimulated for 24- and 48-hours with anti-CD3/28 and treated with vehicle (DMSO), SPRi3 (50μM) and Sepiapterin (5μM). Experiment was repeated two independent times with similar results. **g, h,** Amino acid profiles in the supernatants (**g**) and the cell pellets (**h**) from 24-hour anti-CD3/CD28 stimulated $CD4^+$ T cells from control and *Gch1;Lck* mice. n=3 for each genotype. Data are shown as means ± s.e.m. NS, not significant (2-tailed, Student's t-test).

Extended Data Figure 5. Mitochondrial dysfunction in BH4-depleted T cells after activation

a, b, ATP measurements in control (n=3) and *Gch1;Lck* (n=3) $CD4^+$ T cells **(a)** and wild type $CD4^+$ T cells treated with DMSO vehicle (n=3) or SPRi3 (50μM, n=3) **(b)** left unstimulated or assayed at the indicated timepoints after T cell activation (anti-CD3/28). Data are shown as means ± s.e.m. n = 3 for each genotype. *P < 0.05; **P < 0.01 (2-tailed, Student's t-test with multiple comparisons). **c,** Metabolomic measurements of lactate and pyruvate levels from cell pellets of 16-hour anti-CD3/28 activated $CD4^+$ T cells from control and *Gch1;Lck* mice. Data are shown as means ± s.e.m. n = 4 for each genotype. *P < 0.05; (2-tailed, Student's t-test). **d,** Routine and total capacitance oxygen respiration in intact, 16-hour anti-CD3/CD28-stimulated $CD4^+$ T cells from control and *Gch1;Lck* mice. Data from individual mice are indicated ± s.e.m. N=4 for each genotype. **P < 0.01 (2-tailed, Student's t-test). **e, f,** Oxygen uptake rate in permeabilized, 16-hour anti-CD3/CD28-stimulated $CD4^+$ T cells from control (n=4) and *Gch1;ROR* (n=4) mice **(e)** and DMSO- and SPRi3-treated (50μM, n=5 each) wild type $CD4^+$ T cells **(f)**. Data from individual mice are indicated ± s.e.m. *P < 0.05; **P < 0.01 (2-tailed, Student's t-test). **g,** Representative oxygen consumption traces (left panel) of complex I-linked and complex II-linked ETC activity from 16-hour activated wild type $CD4^+$ T cells treated with vehicle or SPRi3 (50μM). Relative Complex I and II-linked activities (right panel) in activated control cells treated with vehicle (n=4) or SPRi3 (50μM, n=4). Data are shown as means ± s.e.m., NS, not significant, *P < 0.05 (2-tailed, Student's t-test).

Extended Data Figure 6. Enhanced superoxide levels independent of iNOS coupling observed in BH4-deficient activated T cells

a, b, Representative FACS histogram **(a)** and quantification of the mean fluorescent intensity (MFI) **(b)** depicting DHE (dihydroethidium, superoxide ROS indicator) levels in unstimulated

and 20-hour anti-CD3/28 activated $CD4^+$ T cells from control, *GCH1;RORc* mice as well as control cells treated with SPRi3 (50μM). n=3 samples per group. Experiment was repeated three independent times showing similar results. **c, d,** Proliferation of control (n=6) and *Gch1;Lck* (n=9) $CD4^+$ T cells and treatment with the superoxide scavenger NAC (N-acetyl-L-cysteine; 500μM, n=4 each)). Representative 3-day proliferation histograms are shown **(c)** and quantification **(d)**. Data are shown as means ± s.e.m. Individual mice for each genotype are shown. ****P < 0.0001 (One-way ANOVA with Tukey's multiple comparison test). **e,** Total iron content from anti-CD3/28 stimulated $CD4^+$ T cells for 24 hours (untreated and treated with 500μM NAC) from control (n=17, 4, respectively) and *Gch1*;*RORc* (n=22, 6, respectively) mice. Data are shown as means ± s.e.m. Individual mice for each genotype are shown. **P < 0.01 (2-tailed, Student's t-test with Tukey's multiple comparisons). **f,** ATP measurements of stimulated wild type $CD4^+$ T cells treated with DMSO, sepiapterin and NAC for 24 hours. Data are shown as means ± s.e.m. n = 5 for each genotype. *P < 0.05; **P < 0.01 (2-tailed, Student's t-test with multiple comparisons). **g,** Intracellular iNOS expression in purified $CD4^+$ control T cells left untreated or anti-CD3/CD28 stimulated for 12, 24 and 72 hours. Experiment was repeated two independent times showing similar results. **h,** Representative histogram showing iNOS expression in control and *Gch1*-ablated $CD4^+$ T cells anti-CD3/CD28 stimulated for 72 hours. Quantification of $iNOS^+$ cells over time. n=4 for each genotype. Data are shown as means ± s.e.m. NS, not significant (2-tailed, Student's t-test). **i,** Nitrite measurements in the supernatant of stimulated cells in **(h).** Peritoneal, thioglycollate-elicited macrophages stimulated with LPS (100ng/ml) for 24 hours were used as a positive control. Data are shown as means ± s.e.m. N=4 for each genotype. NS, not significant (2-tailed, Student's t-test).

Extended Data Figure 7. Functional evaluation of the SPR blocker, QM385

a, Schematic of the BH4 pathway indicating the mode of action for QM385 on SPR, thereby limiting BH4 production and correspondingly increasing sepiapterin levels that can be used as a biomarker for QM385-mediated SPR inhibition. **b, c,** A Representative concentration-response curve of QM385 binding affinity to human SPR tested *in vitro* by time-resolved fluorescence resonance energy transfer assay (TR-FRET) **(b)** and reduction of BH4 levels upon QM385 treatment in anti-CD3/28-stimulated mouse splenocytes (left panel, 2 independent experiments) and human PBMCs (right panel, 2 independent experiments) levels **(c)**. Indicated in red are the calculated IC_{50} values for each assay. Binding effect assay was repeated 162 independent times with similar results. **d,** Oxygen uptake rate in permeabilized, 16-hour anti-CD3/CD28-stimulated wild type $CD4^+$ T cells treated with DMSO or QM385 (2.5μM). Data from individual mice (n=3) are indicated ± s.e.m. ***P < 0.001 (2-tailed, Student's t-test). **e,** ATP measurements of unstimulated (n=8) and 24-hour activated wild type $CD4^+$ T cells treated with DMSO vehicle (n=4) or varying doses of QM385 (n=4 for each dose). Data are shown as means ± s.e.m. NS, not significant; **P < 0.01 (One-way ANOVA with Dunnett's multiple comparisons). **f,** Fold changes in DHE levels (superoxide ROS indicator) between DMSO-treated and QM385-treated (2.5μM) 20-hour activated $CD4^+$ T cells. Data from individual mice (n=4) are indicated ± s.e.m. **P < 0.01 (2-tailed, Student's t-test). **g,** Allergic airway inflammatory disease model and quantification of inflammatory cells in bronchoalveolar lavage fluids (BALFs). Data are shown

as box and whisker (running from minimal to maximal values) plots for which individual data points are shown. n=15 for vehicle-treated mice; n=17 for QM385-treated mice. QM385 (1mg/kg) was administered orally (PO) twice a day for 3 consecutive days as depicted in the schematic. *P < 0.05; **P < 0.01 (2-tailed, Student's t-test). **h,** Human $CD4^+$ T cell proliferation from 2 donors performed in triplicate samples. Anti-CD3/28 T cells were stimulated with varying doses of QM385 and total counts were measured. Data are shown as means ± s.e.m. **P < 0.01, P < 0.05 (One-way ANOVA with Dunnett's multiple comparisons).

Extended Data Figure 8. Increased effector T cells in naïve mice overexpressing *Gch1* and enhanced T cell proliferation after stimulation

a, Representative immunoblot to detect GCH1 and the HA tag in naïve $CD4^+$ T cells from control and *GOE;Lck* overexpressing mice. Experiments was repeated three times with similar findings. **b, c,** Proportion of splenic T and B cells **(b)** as well as the proportion of $CD4^+$ and $CD8^+$ T cells among the splenic T cell ($TCR\beta^+$) population **(c)** from control (n=4) and *GOE;Lck* (n=4) mice. Data of individual mice aged 8 weeks are shown as means ± s.e.m. NS, not significant. (2-tailed, Student's t-test). **d,** Quantification of naïve ($CD44^{lo}$; $CD62L^{hi}$), memory ($CD44^{hi}$; $CD62L^{hi}$) and effector ($CD44^{hi}$; $CD62L^{lo}$) T cell subtypes from the spleen of control (n=6) and *GOE;Lck* (n=10) mice. Data of individual mice are shown as means ± s.e.m. **P < 0.01; ***P < 0.001; NS, not significant (2-tailed, Student's t-test). **e,** Cell numbers of B cells, T cells as well as $CD4^+$ and $CD8^+$ T cells in the spleens of control and *GOE;CD4* mice. Data from individual mice (n=4 for each genotype) are shown as means ± s.e.m. NS, not significant. (2-tailed, Student's t-test). **f,** Proportion of $CD4^+$ and $CD8^+$ naïve, memory, and effector T cells in the spleens of naïve control and *GOE;CD4* mice. Data of individual mice mice (n=4 for each genotype) are shown as means ± s.e.m. *P < 0.05; **P < 0.01; ***P < 0.001; NS, not significant (2-tailed, Student's t-test). **g,** Representative histograms depicting dose-dependent proliferation of anti-CD3/28 stimulated $CD4^+$ T cells for 3 days from control and *GOE;CD4* mice. Experiments were repeated >3 times showing comparable results. **h,** IL-2 and IFNγ secretion after three days of $CD4^+$ T cell activation (anti-CD3/28) from control and *GOE;CD4* mice. Data are shown as means ± s.e.m. n = 3 for each genotype. *P < 0.05; ***P < 0.0001 (2-tailed, Student's t-test). **i, j,** Quantification of $CD4^+$ T cell proliferation **(i)** and cytokine secretion **(j)** after 3 days of anti-CD3/28 stimulation from control (n=3) and *GOE;ERT* (n=3) mice treated with 4-hydroxytamoxifen (4-OHT, 0.5μM) to induce *Gch1* overexpression *in vitro*. Data from individual mice are shown as means ± s.e.m. **P < 0.01; ***P < 0.001 (2-tailed, Student's t-test).

Extended Data Figure 9. T cells overproducing BH4 display enhanced ATP production, proliferation and autoimmunity

a, Allergic airway inflammatory disease model and fold change of inflammatory cells in bronchoalveolar lavage fluids (BALFs) comparing control and *GOE;Lck* mice. Data are shown as means ± s.e.m. n=18 for control mice; n=17 for *GOE;Lck* mice. *P < 0.05; **P < 0.01 (2-

tailed, Student's t-test). **b,** Transfer colitis model. Changes in body weight of *Rag2* KO mice transferred with control (n=6) and *GOE;CD4* (n=5) naïve $CD4^+$ T cells. Data are shown as means ± s.e.m. *P < 0.05; ***P < 0.001 Data are shown as means ± s.e.m. *P < 0.05; ***P < 0.001; NS, not significant (Two-way ANOVA with Tukey's multiple comparison test). **c,** Total numbers of activated ($CD62L^{low}$; $CD44^{high}$) $CD4^+$ splenic T cells at 3 weeks post-transfer in mice transferred with control and *GOE;CD4* naïve $CD4^+$ T cells. Data for two mice of each group are shown. **d,** Naive $CD4^+$ T cell transfer (150,000 cells) colitis model with co-transfer of FACS-purified Treg cells from control (n=5) and *GOE;CD4* (n=6*)* mice. Changes to initial body weights (BW) were scored over 7 weeks. Data are shown as means ± s.e.m. ***P < 0.001; NS, not significant (Two-way ANOVA with Tukey's multiple comparison test). **e,** Representative histograms depicting purified unstimulated and anti-CD3/28 stimulated $CD4^+$ and $CD8^+$ wild type and *Gch1;RORc* T cell proliferation after 3 days treated with Sepiapterin (5μM). The profile for the unstimulated T cells of each genotype is shown in grey. Experiments were repeated 3 independent times showing comparable results. **f, g,** Representative FACS plot of EdU cell-cycle analysis after 28-hours anti-CD3/28 stimulation of control, *GOE;CD4*, control treated with SP (5μM), and *GCH1;RORc* treated with SP (5μM) $CD4^+$ T cells **(f)** and quantification of the S-phase entry population **(g)**. EdU was pulsed for the last 4 hours of stimulation. N=4 mice for control; n=3 mice for all other genotypes. ***P < 0.001 (One-way ANOVA with Dunnett's multiple comparisons test). **h, i,** Effect of BH4 on T cell proliferation (^3H thymidine incorporation; **h**) and IL-2 secretion **(i)** of $CD4^+$ wild type T cells activated with anti-CD3/28 for 24 hours and treated with vehicle (n=3/4) or BH4 (10μM, n=3/4). Data are shown for individual mice as means ± s.e.m. **P < 0.01 (2-tailed, Student's t-test). **j,** Representative histograms depicting proliferation of control and *Gch1;RORc* $CD4^+$ T cells after 3 days of anti-CD3/28 stimulation which were supplemented with BH4 (10μM). FACS blots are representative of two independent experiments showing comparable results.

Extended Data Figure 10. Overactivation of the GCH1/BH4 pathway leads to enhanced anti-tumor immunity.

a, Total iron content from 24-hour anti-CD3/28 stimulated $CD4^+$ T cells (untreated and treated with 5μM sepiapterin) from control (n=5) and *Gch1*;*RORc* (n=5) mice. Data are shown as means ± s.e.m. individual mice for each genotype are shown. *P < 0.05 (One-way ANOVA with Tukey's multiple comparisons. **b,** Representative FACS histogram depicting DHE (superoxide ROS indicator) levels (left panel) and quantification of the mean fluorescent intensity (right panel) in unstimulated and anti-CD3/28 activated $CD4^+$ T cells for 20 hours from control and *GOE;CD4* littermates as well as wild type cells treated with Sepiapterin (5μM). N=3 for each condition. Data are shown as means ± s.e.m. **P < 0.01; ***P < 0.001 (One-way ANOVA with Tukey's multiple comparisons test). **c,** ATP measurements of stimulated wild type $CD4^+$ T cells treated with DMSO, sepiapterin (5μM) and SPRi3 (50μM) for 24 hours. Data are shown as means ± s.e.m. n = 3 for each genotype. *P < 0.05; **P < 0.01 (2-tailed, Student's t-test with multiple comparisons). **d,** Quantification of intratumoral effector $CD4^+$ T cells ($CD44^+CD62L^{lo}$) assayed from E0071 tumors on day 28 of vehicle and BH4-treated mice. Data are shown as

means ± s.e.m. N=5 mice for each condition. *P < 0.05; **P < 0.01 (2-tailed, Student's t-test). **e,** Effect of BH4 supplementation on HRas-transformed TC-1 tumor growth. TC-1 tumor cells were orthotopically injected and once the tumors were palpable (day 7), BH4 (35mg/kg, n=15) or vehicle (saline, n=10) were therapeutically administered for 7 days as indicated. Data are shown for individual mice as means ± s.e.m. ***P < 0.001; ****P < 0.0001 (Two-way ANOVA with Sidak's multiple comparisons). **f,** Quantification of intratumoral effector $CD8^+$ T cells ($CD44^+CD62L^{lo}$) assayed from TC-1 tumors on day 21 of vehicle and BH4-treated mice (n=9 mice for each genotype). Data are shown as means ± s.e.m. **P < 0.01 (2-tailed, Student's t-test). **g,** Effect of BH4 supplementation on TC-1 tumor growth in *Rag2* KO hosts. TC-1 tumor cells were orthotopically injected into *Rag2* KO female mice and once the tumors were palpable (day 7), BH4 (35mg/kg, n=5) or vehicle (saline, n=5) were administered. BH4 and vehicle supplementation was carried out for 7 days as indicated on the graph. Data are shown for individual mice as means ± s.e.m., NS, not significant. (Two-way ANOVA with Sidak's multiple comparisons). **h,** Sepiapterin levels in the supernatant of wild type $CD4^+$ T cells stimulated with anti-CD3/28 for 20 hours treated with vehicle and kynurenine (KYN, 150μM). Culture media was also included for comparison. BQL, below quantifiable levels. Data are shown as means ± s.e.m. N=4 independent samples for each condition. ***P < 0.001 (One-way ANOVA with Tukey's multiple comparisons test). **i,** Representative histogram depicting proliferation of 3-day anti-CD3/28 activated wild type $CD4^+$ T cells treated with vehicle or kynurenine (50μM). **j,** Representative FACS histograms depicting DHE (superoxide ROS indicator) levels in anti-CD3/28 stimulated wild type $CD4^+$ T cells treated with vehicle (DMSO), kynurenine (KYN) alone (50μM) or KYN (50μM) plus BH4 (10μM) for 20 hours. Experiment was repeated three independent times showing comparable results.

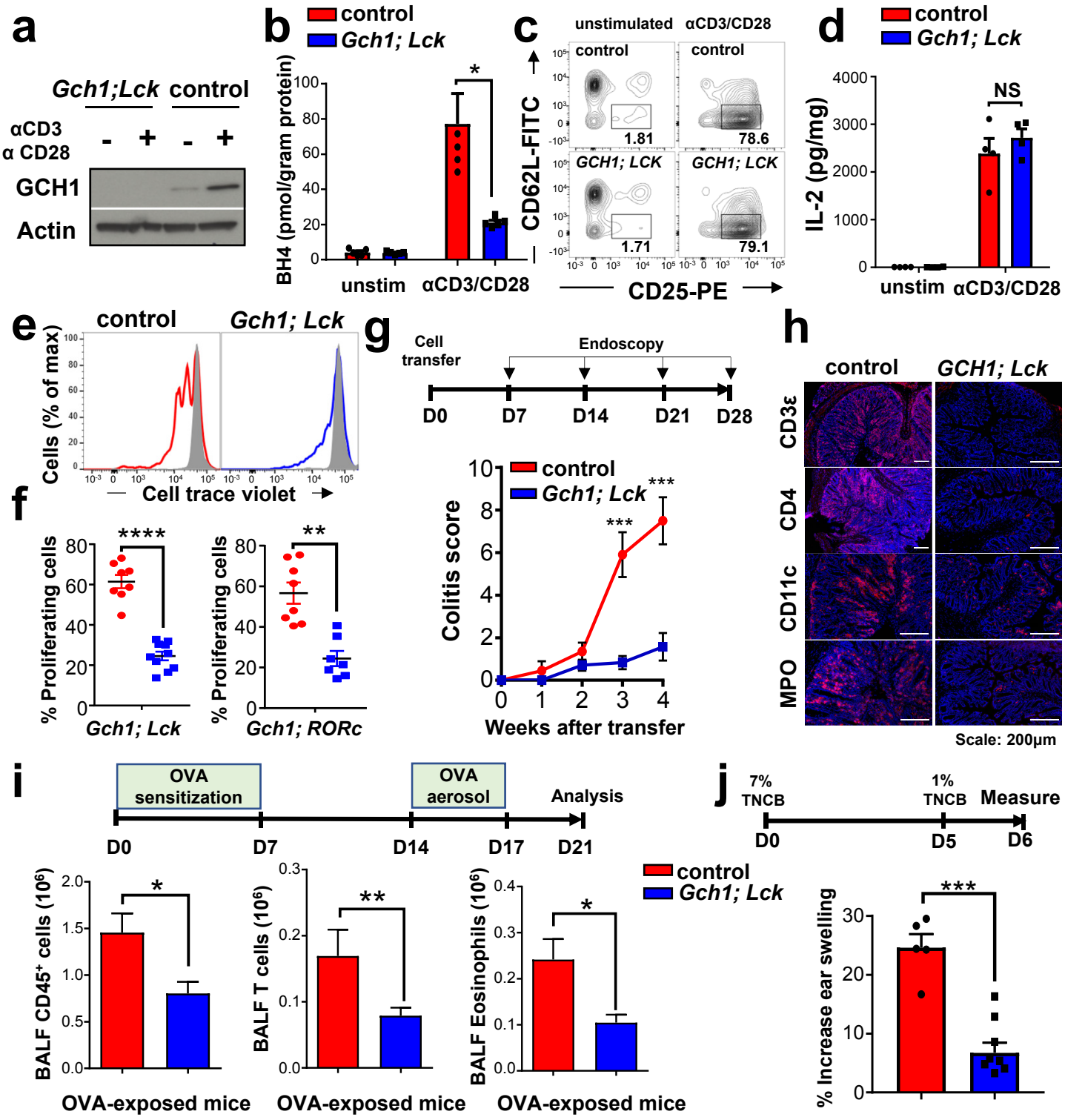
a
Gch1;Lck
control
αCD3
α CD28
GCH1
Actin
b
control
Gch1; Lck
BH4 (pmol/gram protein)
unstim
αCD3/CD28
c
unstimulated
αCD3/CD28
control
GCH1; LCK
CD62L-FITC
CD25-PE
1.81
78.6
1.71
79.1
d
IL-2 (pg/mg)
NS
e
Cells (% of max)
Cell trace violet
f
% Proliferating cells
Gch1; Lck
Gch1; RORc
g
Cell transfer
Endoscopy
D0
D7
D14
D21
D28
Colitis score
Weeks after transfer
h
CD3ε
CD4
CD11c
MPO
Scale: 200μm
i
OVA sensitization
OVA aerosol
Analysis
BALF CD45⁺ cells (10⁶)
BALF T cells (10⁶)
BALF Eosinophils (10⁶)
OVA-exposed mice
j
7% TNCB
1% TNCB
Measure
% Increase ear swelling

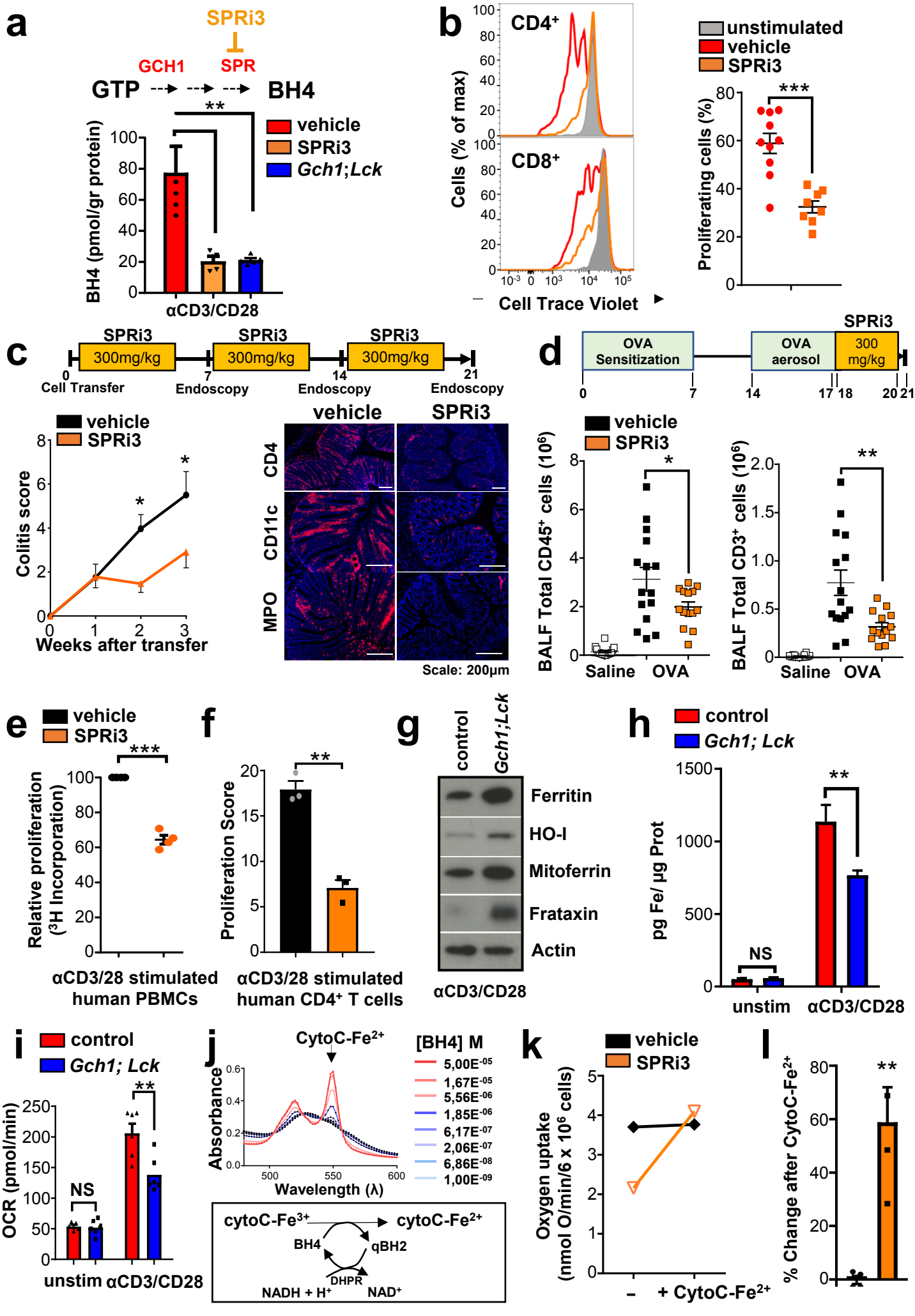
a
SPRi3
GCH1
SPR
GTP
BH4
**
vehicle
SPRi3
Gch1;Lck
BH4 (pmol/gr protein)
αCD3/CD28
b
CD4+
CD8+
Cells (% of max)
Cell Trace Violet
unstimulated
vehicle
SPRi3
***
Proliferating cells (%)
c
SPRi3
300mg/kg
Cell Transfer
Endoscopy
Endoscopy
Endoscopy
vehicle
SPRi3
Colitis score
Weeks after transfer
CD4
CD11c
MPO
Scale: 200μm
d
OVA Sensitization
OVA aerosol
SPRi3
300 mg/kg
BALF Total CD45+ cells (10^6)
BALF Total CD3+ cells (10^6)
Saline
OVA
e
Relative proliferation (3H Incorporation)
αCD3/28 stimulated human PBMCs
f
Proliferation Score
αCD3/28 stimulated human CD4+ T cells
g
control
Gch1;Lck
Ferritin
HO-I
Mitoferrin
Frataxin
Actin
αCD3/CD28
h
control
Gch1; Lck
pg Fe/ μg Prot
NS
unstim
αCD3/CD28
i
control
Gch1; Lck
OCR (pmol/min)
NS
unstim
αCD3/CD28
j
CytoC-Fe2+
Absorbance
Wavelength (λ)
[BH4] M
5,00E-05
1,67E-05
5,56E-06
1,85E-06
6,17E-07
2,06E-07
6,86E-08
1,00E-09
cytoC-Fe3+
cytoC-Fe2+
BH4
qBH2
DHPR
NADH + H+
NAD+
k
vehicle
SPRi3
Oxygen uptake (nmol O/min/6 x 10^6 cells)
–
+ CytoC-Fe2+
l
% Change after CytoC-Fe2+

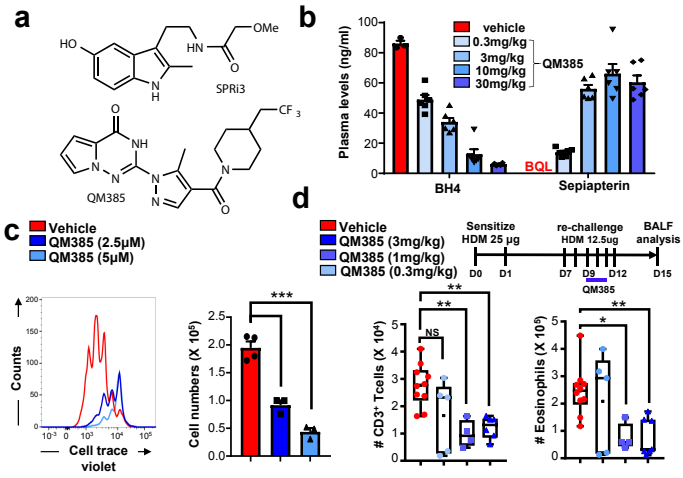
a
HO
HN
OMe
O
N
H
SPRi3
O
NH
N
N
N
N
CF 3
N
O
QM385
b
Plasma levels (ng/ml)
vehicle
0.3mg/kg
3mg/kg
10mg/kg
30mg/kg
QM385
BQL
BH4
Sepiapterin
c
Vehicle
QM385 (2.5μM)
QM385 (5μM)
Counts
Cell trace violet
Cell numbers (X 10⁵)
***
d
Vehicle
QM385 (3mg/kg)
QM385 (1mg/kg)
QM385 (0.3mg/kg)
Sensitize HDM 25 μg
re-challenge HDM 12.5ug
BALF analysis
D0
D1
D7
D9
D12
D15
QM385
CD3⁺ Tcells (X 10⁴)
NS
**
Eosinophils (X 10⁵)
*

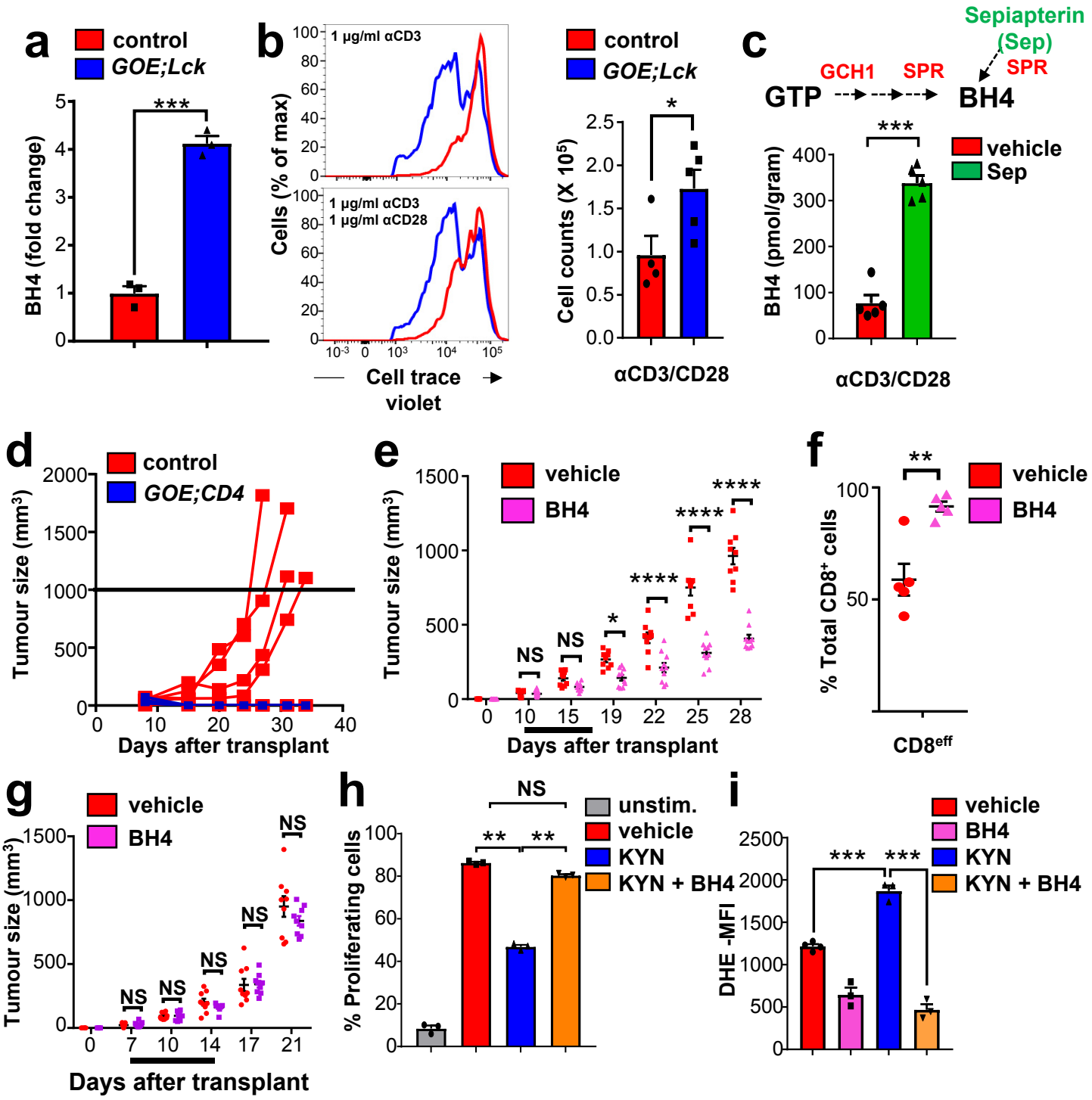
a
control
GOE;Lck
BH4 (fold change)
***
b
1 µg/ml αCD3
1 µg/ml αCD3
1 µg/ml αCD28
Cells (% of max)
Cell trace violet
control
GOE;Lck
Cell counts (X 10⁵)
*
αCD3/CD28
c
Sepiapterin (Sep)
GCH1
SPR
SPR
GTP
BH4
***
vehicle
Sep
BH4 (pmol/gram)
αCD3/CD28
d
control
GOE;CD4
Tumour size (mm³)
Days after transplant
e
vehicle
BH4
Tumour size (mm³)
NS
NS
*
****
****
****
Days after transplant
f
**
vehicle
BH4
% Total CD8⁺ cells
CD8eff
g
vehicle
BH4
Tumour size (mm³)
NS
NS
NS
NS
NS
Days after transplant
h
NS
**
**
unstim.
vehicle
KYN
KYN + BH4
% Proliferating cells
i
***
***
vehicle
BH4
KYN
KYN + BH4
DHE -MFI